JPL PUBLICATION 79-117

Radio Propagation Through Solar and Other Extraterrestrial Ionized Media

Ernest K. Smith
Robert E. Edelson

January 15, 1980

National Aeronautics and
Space Administration

Jet Propulsion Laboratory
California Institute of Technology
Pasadena, California

JPL PUBLICATION 79-117

Radio Propagation Through Solar and Other Extraterrestrial Ionized Media

Ernest K. Smith
Robert E. Edelson

January 15, 1980

National Aeronautics and
Space Administration

Jet Propulsion Laboratory
California Institute of Technology
Pasadena, California

FOREWORD

This report was originally intended to be a United States contribution to the work of Study Group 6 (propagation in ionized media) of the International Radio Consultative Committee (CCIR). The area of Extraterrestrial propagation is a new one to Study Group 6 (see Appendix A) so it was felt that a fairly substantial contribution was indicated. However, when completed, the report was too long to be included in its entirety, and Section II was deemed too mathematical. Upon suggestion from Dr. Rush (chairman of U.S. Study Group 6) it was decided to reproduce the full report as a JPL Publication.

It is a pleasure to acknowledge the generous assistance of the following individuals (listed alphabetically) who provided useful data or helpful comments:

John W. Armstrong
Allen L. Berman
Henry G. Booker
Jay C. Breidenthal
Norman E. de Groot
Charles Elachi
Bruce E. Goldstein
John M. Kelso
Murray A. Koerner
Tomas A. Komarek
Boyd Madsen
R. P. Mathison
Marcia M. Neugebauer
Lawrence L. Rauch
Boris Seidel
Charles T. Stelzried
Bruce T. Tsurutani
Richard T. Woo
Sien Wu

ABSTRACT

The International Radio Consultative Committee (CCIR), in response to a U.S. initiative, approved a new Study Programme in 1978 entitled, "Radio propagation through the solar and other extra-terrestrial ionized media." The work described in the present report was carried out in response to the CCIR call for contributions in this area. It is intended for engineers with some background in radiowave propagation and frequency allocations.

The report first treats the present S- and X-band communications needs in deep space to illustrate the aspects which are affected by propagation through extraterrestrial plasmas, and develops (in Table III) the magnitude, critical threshold, and frequency dependence of some eight propagation effects for an S-band propagation path passing within 4 $R_\odot$ of the Sun.

The second section deals with the theory and observation of propagation in extraterrestrial plasmas. The various plasma states along a near-solar propagation path are illustrated. Classical magneto-ionic theory (cold anisotropic plasma) is examined for its applicability to the path in question. Table IV summarizes the characteristics of the plasma states found along the path and indicates the errors in some of the standard approximations.

The third section, on models of extraterrestrial plasmas, is primarily directed towards modelling the electron density in the solar corona and solar wind, but does also offer some cursory information on the terrestrial planets plus Jupiter.

CONTENTS

Figures

Tables

SECTION I

PROPAGATION EFFECTS IN DEEP SPACE COMMUNICATIONS THROUGH EXTRATERRESTRIAL PLASMAS

1. INTRODUCTION

The effects produced by ionized media beyond the Earth's ionosphere on radio propagation are important in the selection of operating frequencies for future deep-space missions. The purposes of this report are twofold: (1) to identify those propagation parameters that are apt to be controlling, or at least significant, in the selection of frequency; (2) to examine those parameters in sufficient detail to assess the magnitude of their change and their behavior as a function of frequency.

To accomplish this, the report contains a consideration of those telecommunications engineering and science requirements of space systems that are most apt to be affected by propagation effects. The magnitude of the propagation effects for a sample case and their behavior as a function of frequency are then tabulated. Theoretical and observational aspects of propagation in plasmas are summarized in Section II and illustrated with examples of propagation through the solar corona and interplanetary medium. Section III considers physical models of the solar corona and solar wind, and presents sample profiles of planetary ionospheres.

One of the major concerns in the deep-space research program has to do with the use of yet higher frequencies (to the neighborhood of 30 GHz) for future deep-space missions. It raises questions both from the standpoint of the performance of the deep-space links considered in isolation, and from the standpoint of frequency allocations and sharing where the needs and characteristics of other services are involved. The Earth's atmosphere including hydrometeors will be a major factor, but its effect on deep-space is not significantly different from the geostationary satellite case. The effect of extraterrestrial ionized media, particularly in the solar corona, is unique to deep-space telecommunications.

2. PROPAGATION EFFECTS RELEVANT TO DEEP-SPACE TELECOMMUNICATIONS

The radio link connecting the Earth and the spacecraft has three primary functions. Telemetry is the first of these and has to do with the transmission of downlink data telling us about the spacecraft's surroundings: for example, video data of a planet's surface. Telemetry is characterized by its volume and the requirement for moderate to high quality data (e.g., a video picture contains enough redundancy that a few errors in data bit detection will not be catastrophic, whereas loss of data on plasma structure would be much more serious). The second function is command, which refers to information sent to the spacecraft from the ground. This information contains directions to the spacecraft to alter its preprogrammed instructions and to take specified action with specified parameters at definite times. Command is characterized by low data volume and a requirement for extreme accuracy. The third function of the radio link is "radiometrics", a term that includes the development of information for navigation and scientific purposes from characteristics of the received radio signals. These characteristics are imposed by the position and velocity of the spacecraft, and by the propagation medium.

Two principal factors serve to alter the radio signals in their passage between Earth and spacecraft: the propagation medium, which may significantly degrade the signal for all three functions, and the velocity of the spacecraft relative to the ground stations. By exceedingly accurate measurements of the radiowave characteristics, the position of the spacecraft, its velocity, and its acceleration can be determined. Simultaneously, information is acquired on the structure, composition, and temperature of the propagation medium (typically the solar corona or the atmosphere of a planet that may occult the signal, or the interplanetary plasma state along the ray path), and on planetary and solar gravitational fields. These radiometric measurements are characterized by the need for a high order of long-term frequency stability (for example, to parts in 10^{15} for the Earth station for gravitational waves), and by the extent of data processing required to turn the signal into information [Edelson et al, 1979].

The performance of these three radio-link functions is dependent on the signal-to-noise ratio (SNR), which may be defined by the equation:

$$P_r/N_o = P_t + G_t + G_r - L_1 - L_2 - 20 \log f - 10 \log d - 10 \log T_s - 27.34 \text{ dB} \quad (1)$$

where

P_t : transmitter power (dbW)

G_t : transmitting antenna gain with respect to an isotropic radiator (dBi)

G_r : receiving antenna gain (dBi)

L_1 : attenuation in propagation medium different from free space (dB)

L_2 : all other losses from receiving antenna to first stage of receiver (dB)

f : frequency (GHz)

d : distance in astronomical units (1 AU = 1.496×10^{11} m)

T_s : system noise temperature including additive noise (K).

An example illustrating the magnitude of these parameters for the case of the NASA Voyager spacecraft at the distance of Jupiter is given in Table I. The locations and diameters of the antennas of the three NASA Deep Space Network (DSN) complexes are shown in Table II. A comparison of the losses incurred simply due to distance, between satellites in geostationary orbit and spacecraft on planetary missions is shown in Figure 1. The nearest of the inner planets is seen to experience 60 dB more loss for any given frequency; the nearest of the outer planets experience 87 dB more loss than for the geostationary case.

Increasing the gain of a parabolic antenna (commonly used for deep-space work) decreases the beamwidth as illustrated in Figure 2 (where the effect of surface irregularities is also portrayed). If there is angular broadening due to plasma effects this may spread the angular spectrum of incoming plane waves to angles outside the 0.3 dB cone of the antenna thereby causing a decrease in signal level of 0.1 dB or greater.

The telecommunications parameters of a typical deep space mission are given in Table I and the antenna locations and dimensions in Table II. While the spacecraft transmitter power is seen to be modest, only 21.3 watts at X-band (8.4 GHz) and 6.6 watts (18.9 watts in the high power mode) at S-band (2.3 GHz), the input power required to generate it represents a substantial fraction of the total spacecraft power.

Phase modulation is used to impress information on the carrier signal, and several components of the single-bit stream are separately coded to achieve the bit-error-rate required for each function or experiment. This scheme is called concatenated coding. In the case of Voyager, it allows a two-orders-of-magnitude BER difference between imaging and nonimaging data. The cost is in increased ground-processing complexity. Only recently have ground computer speeds increased to the point where decoding of concatenated coding becomes feasible.

Criteria for determining just what constitutes a significant change in a propagation parameter are not easily established. A case in point might be broadening of the carrier signal that is used to synchronize the receiving system on the ground. The phase lock loop has a bandwidth of tens of Hertz (function of received power), so that broadening of the carrier by plasma fluctuations to say 50 Hertz could cause loss of lock, if the received power level were to be decreased simultaneously by amplitude scintillation.

Similarly with the telemetry signal, if the margin has been exhausted, a further decrease of SNR by 0.7 dB will cause a ten-fold increase in imaging error rate, and 1000-fold for nonimaging error rates (assuming curves 3 and 4 of Figure 3 for inner and outer coding, respectively). Error considerations in deep-space telecommunication systems are governed by the error source with the largest standard deviation. At the present time an uncertainty of 0.1 dB is significant.

2.1 Radio Science

In general, the effects produced by plasma on communications are undesirable. However, in radio-science investigations, these plasma effects while at times undesirable, as in the case of very precise celestial mechanics measurements are, at other times, used to develop information about the propagation media. Both situations deserve comment.

TABLE I

Typical NASA Voyager Telecommunications Parameters

Parameter	Unit	Value		
		Telemetry		
		X-band	S-band	Command
Carrier frequency, f	Gigahertz	8.4	2.3	2.1
Transmitter power, P_t	dBW	13.3	8.2†	40.0
Antenna gain, G_t	dBi	48.1	35.1	60.79
Range at Jupiter, d	AU	4.55	4.55	4.55
Receiving antenna diameter, D	m	64.0	64.0	3.7
Receiving antenna effective gain, G_r	dBi	70.2	61.6	33.7
System losses, L_1+L_2	dB	0.8	0.4	0.0
System noise temperature, T_s	K	28.5	22.3	1500.0
Power flux density at receiving antenna, F	$dB(W/m^2)$	-186.2	-204.4	-147.0
Signal-to-noise ratio, P_r/N_o*	dB(Hz)	58.1	43.6	55.7

*115.2 kilobits per second requires a P_r/N_o of 53.2 dB for a BER of 5×10^{-3}. The 16 b/s command channel requires a P_r/N_o of 35.5 dB for the required command bit error rate of 5×10^{-6}.

†The S-band transmitter power for the high-power mode is 12.8 dBW.

TABLE II

Antennas of the Deep Space Network (DSN)

Location	DSN No.	Antenna Size (m)	Frequencies*
Canberra, Australia			
Tidbinbilla	42	26	S-band
Tidbinbilla	43	64	S-, X-band
Honeysuckle Creek	44	26	S-band
Madrid, Spain			
Robledo	61	26	S-band
Robledo	62	64	S-, X-band
Cebreros	63	26	S-band
Goldstone, California			
Pioneer	11	26	S-band
Echo	12	34	S-, X-band
Mars	13	64	S-, X-band

*S-band frequencies in deep-space use are 2100-2120 MHz uplink, and 2270-2300 MHz downlink;
X-band downlink frequencies are 8400-8440 MHz.

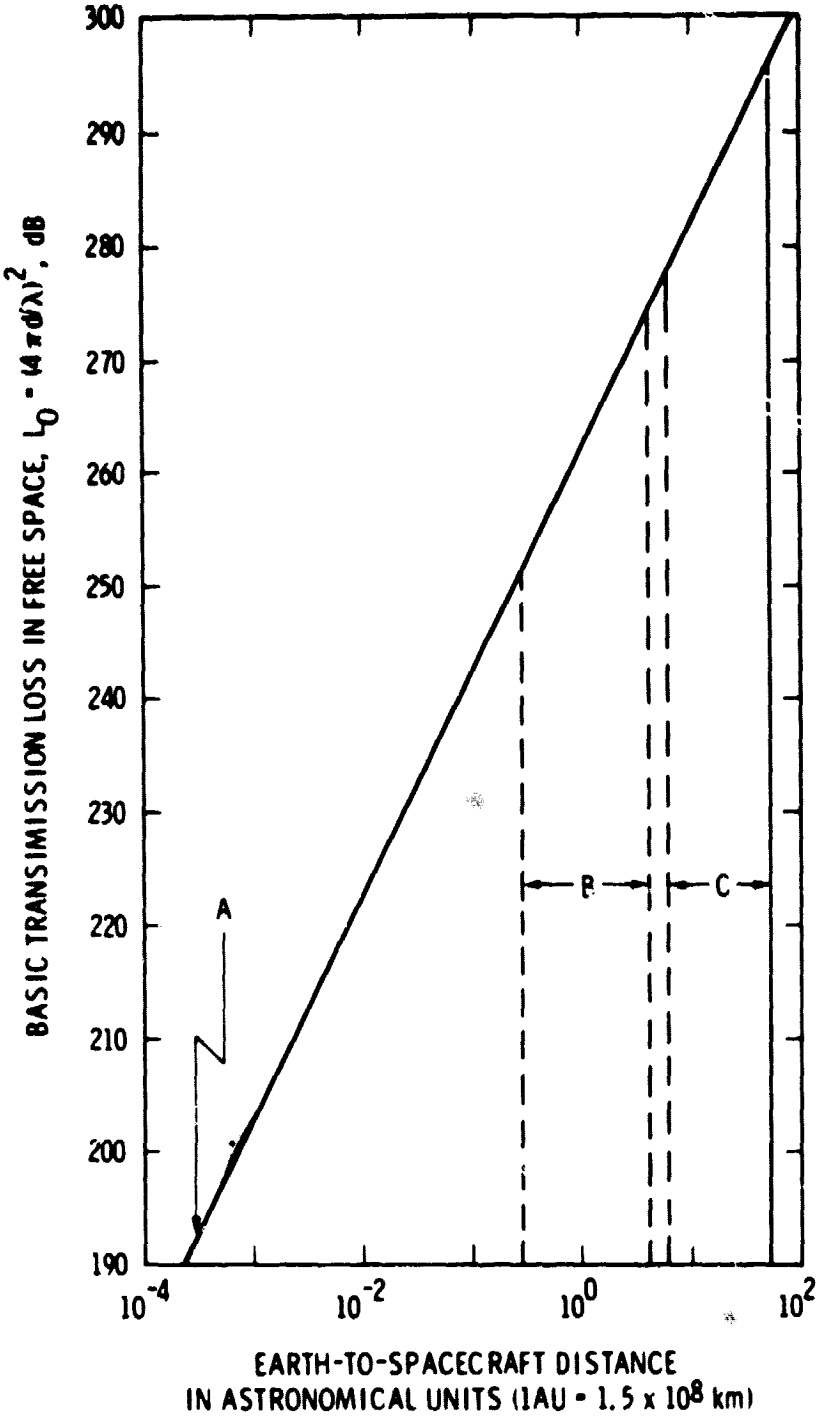

FIGURE 1

Magnitude of basic transmission loss in free space for deep-space telecommunication distances. A = Geostationary distance, B = range of distances to inner planets, C = range of distances to outer planets.

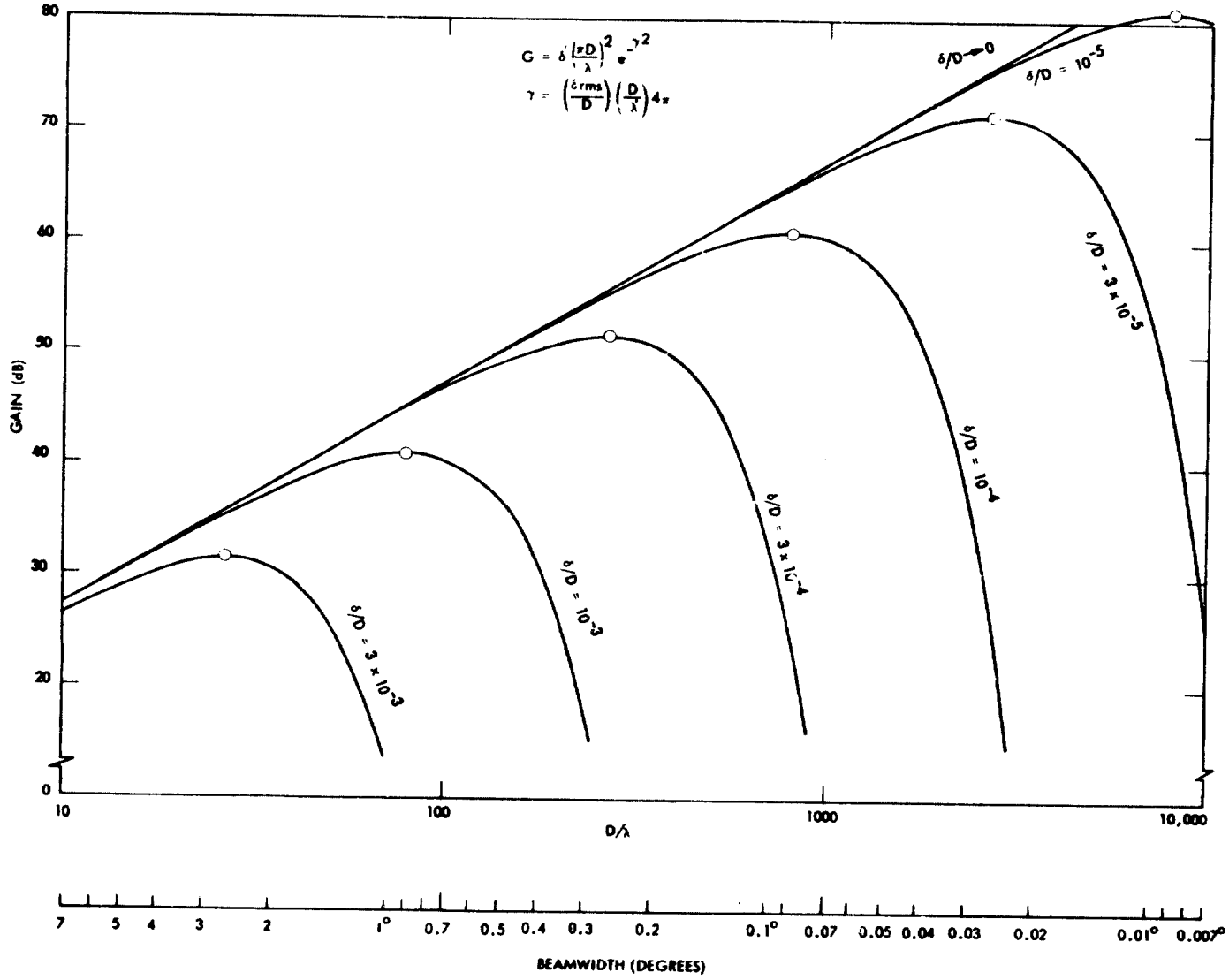

FIGURE 2

Gain and beamwidth as a function of antenna diameter (D) measured in wavelengths (λ) for a parabolic antenna for various cases of δ/D = constant where δ is the value of RMS surface irregularities.

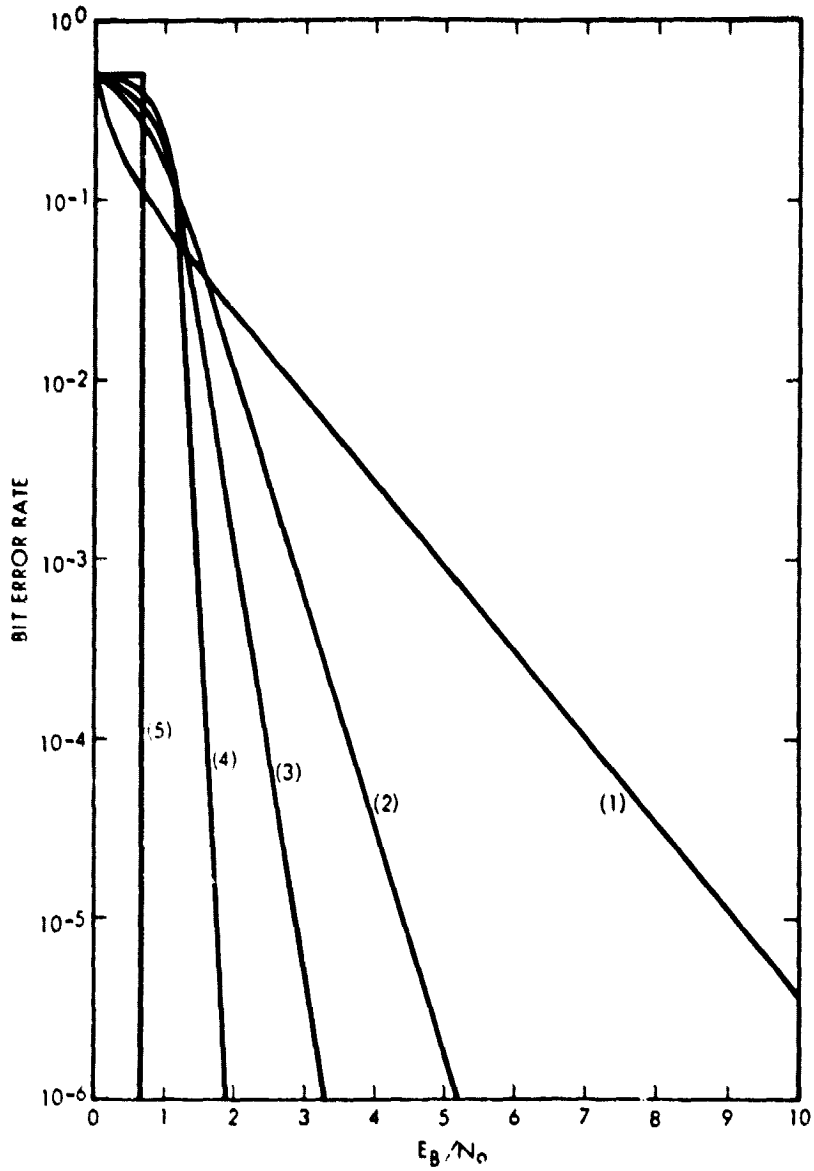

FIGURE 3

Bit error rate associated with different methods of encoding or adding redundancy to transmitted data plotted as a function of signal energy per bit (E_b), divided by noise spectral density (N_o). (After Edelson et al, 1979)

(1) uncoded case,
(2) code used in NASA missions 1969-1976.
(3) NASA Voyager imaging code (inner code).
(4) Voyager non-imaging science concatenated code (combined inner and outer codes).
(5) Theoretical upper bound on performance improvement (infinite bandwidth case), Shannon's limit.

2.1.1 Celestial Mechanics

The effects of gravity on a spacecraft orbit causes detectable changes, which are used for harmonic analysis of the gravitation field of the planet. These analyses can then be interpreted in geophysical terms and related to the internal structure of the planet.

On a more esoteric level gravitational waves are predicted by Einstein's general theory of relativity. If non-gravitational wave fluctuations on the received frequency can be kept below 1 part in 10^{-15}, then it should be possible to detect gravitational waves of a 10^{3}-second duration or longer, assuming time standards of at least this accuracy are available. Either plasma effects on the phase velocity need to be reduced below these levels, or a way needs to be found to determine the extent of the plasma contribution.

General relativity also predicts a decrease in the group velocity of a radio wave due to gravity as it passes close to a massive object such as the Sun or Jupiter. This increase in apparent range is one incentive for improving measurement of apparent range to decimeter or centimeter accuracies at distances of several AU.

2.1.2 Plasma Measurements

Two types of plasma information are derived from the telecommunication (or special beacon) signals. The first is from the spectral broadening, polarization change, phase and amplitude scintillations, and angular broadening. These measurements are all concerned with fluctuations in the plasma. The second, having to do with bulk properties includes information on total electron content which is derived from range and doppler data and Faraday rotation measurements which have been used to gain information on magnetic fields. The principal targets for these measurements are the solar corona, the solar wind, and planetary ionospheres.

Spectral broadening and phase scintillations are two of the most useful radio scattering phenomena that can be observed with monochromatic, coherent, and point source spacecraft signals. Spectral broadening is only useful near the Sun where the induced broadening exceeds the inherent line width of the radio system, which is typically 0.2 Hz. Since spectral broadening measures frequencies higher than 0.2 Hz, it provides information only on the smaller scales of the inhomogeneity spectrum (as also do amplitude scintillations, e.g., Jokipii [1973]). Phase (doppler) scintillations, however, provide information on the full range of scale sizes.

Section II contains a discussion of these effects; also, a good and readable description of these topics is found in Woo [1977].

2.2 Telemetry

The most critical telemetry parameter in practice is signal-to-noise ratio, and for that reason it is worth examining in some detail. Shown in Figure 3 are the bit error rates associated with different methods of encoding data where the abscissa scale is energy per bit (E_B) divided by noise spectral density (N_0). The energy per bit is the received power P_r times the bit duration T_B. In the case of a modern mission such as NASA's Voyager, the error sensitive data is protected by an outer code before being combined with error-insensitive data and put through the inner

encoder. The resultant is satisfactorily robust, and mission requirements are satisfied by E_B/N_o = 2 or 3 dB. However, the bit error rate decays rapidly on both curves 3 and 4 of Figure 3 and this situation changes from sublime to intolerable if the SNR decreases by 2 dB.

Good engineering practice dictates the provision of a power margin. In conventional satellite systems the power margin represents a reserve capacity that is not available to space systems which are stretched to their observing limit. Therefore, there is an argument for not considering the margin in determining the effect of a decrease in signal level due to propagation factors.

Let the criterion for serious deterioration of signal quality be a decade increase in bit error rate at the limiting threshold. For imaging telemetry this threshold is at a BER of 10^{-3}. From Figure 3 curve 3 a change from a BER of 3×10^{-4} to 3×10^{-3} is caused by 0.66 dB decrease in E_B/N_o. Similarly, for nonimaging telemetry (curve 4), the corresponding decade change in BER around 10^{-5} is caused by a 0.19 dB decrease in E_B/N_o.

2.3 Navigation

Interplanetary navigation is consistent with traditional navigation in that it involves a map, a travel plan, a means of periodically determining the ship's location and course, and a method of selecting a new route when the ship has drifted off course. The map of the solar system is constantly being refined. Missions to near and remote planets are planned and spacecraft trajectories determined. The location and velocity (six numbers) of the spacecraft are determined en route (by radio means), and, as a result, corrections are made that allow the spacecraft to reach its interplanetary goal.

The map of the solar system has been materially improved by planetary radar measurements. As late as 1960, the astronomical unit, the mean Sun-Earth distance, was in error by 66,000 km. The present value of 149,597,871 km is known with an uncertainty of about 1 km [Melbourne, 1976]. Radar range measurements of the terrestrial planets are accurate to about 50 meters under favorable conditions.

Two methods for establishing the position and velocity of a spacecraft have been used long enough to be termed classical: the measurement of the round-trip travel time of a radio signal (range), and the measurement of the Doppler shift of the radio wave after it makes the round-trip to the spacecraft and back to Earth (rate of change of range, or radial velocity).

2.3.1 Range

The ranging system presently employed for NASA deep-space missions switches the phase of an S-band carrier back and forth by a radian, say, every microsecond. This is equivalent to a 0.5 MHz square-wave phase modulation. A microsecond corresponds to 300 m, one way, or 150 m range; and it is necessary to decide which 150 meters contains the spacecraft (i.e., there is an ambiguity modulo of 150 m). This is done by successively halving the modulating frequency up to 20 times until the ambiguity is clearly resolved.

Range accuracy by the "classical" method has been about 3 meters in one way range [Melbourne, 1976]. Through careful consideration of the various error factors 1 to 2 meter range accuracy has been achieved at S-band in the present NASA Deep Space Network (DSN). Further improvement in S-band ranging for the inner planets is limited by solar plasma scintillation [Anderson and Estabrook, 1979].

A long-range plan is to move to X-band for ranging. The expectation is that 50 cm ranging at Jupiter distance will be available in ten years, and 10 cm ranging at a later date. This improvement is based on the wider bandwidth available at X-band and the expected f^{-2} decrease in plasma effects at 8.4 GHz as compared to 2.2 GHz.

2.3.2 Range change

A radio signal of frequency f_o sent to a spacecraft from the ground, turned around by the spacecraft transponder, and retransmitted to Earth would arrive with a frequency f_1 which is given by $f_o - f_1 = (V_r/c)2fo$, (typically $f_o - f_1 \sim 100$ kHz), where V_r is the radial velocity of the spacecraft measured in the outward direction; in this example, it is 7.5 km/s. If the frequency can be determined to 0.01 Hz, velocity can be determined to 0.75 mm/s. The actual measurement is in terms of phase and the accuracy depends on the integration time.

These two values of range and range change are quite adequate for navigation in one dimension. A problem arises with respect to the other two coordinates in the plane orthogonal to the radial direction, namely declination and right ascension on the celestial sphere. Here the accuracy of range is not much help. For example, with a spacecraft at a distance of 0.4 AU, a displacement of 600 km perpendicular to the Earth-spacecraft direction results in an increase of only 3 meters in range. As a consequence, a different family of techniques has been developed to determine position and velocity in the plane perpendicular to the radial direction.

2.3.3 Angle determination

Differenced range is a method employed in the NASA Deep-Space Network. Its features are illustrated in Figure 4 where $A_p = B \sin \delta$ is the differential range. As shown in Table II DSN complexes are located in California, Australia and Spain. The U.S. and Australian complexes are located at approximately equal north and south latitudes but differ in longitude by about 90°. Hence the angle measured by differenced range has a large right ascension component as well as a large declination component. As only one tracking station can be transmitting to a spacecraft at a time, simultaneity is actually impossible. Instead the range measurements are "nearly simultaneous." For example in the case of a Saturn conjunction Goldstone, California and Canberra, Australia have the spacecraft in both antenna beams for 4-1/2 hours. The round trip transit time for a radio wave to Saturn and back is 3 hours leaving 1-1/2 hours when either station can command the spacecraft and still receive a response back. During that period command is handed back and forth several times from Goldstone to Canberra in order to achieve near simultaneity.

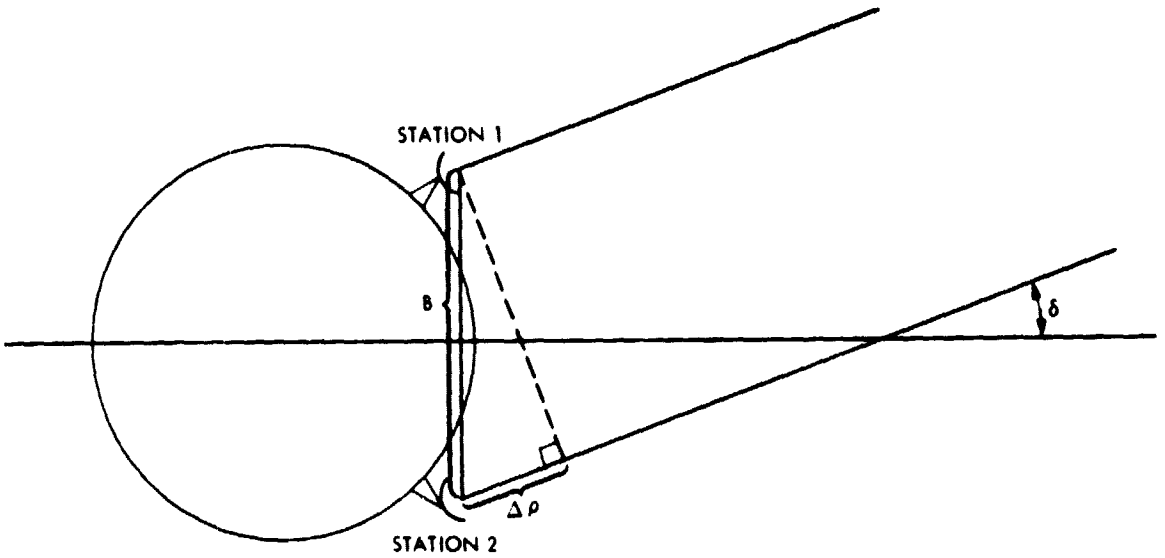

FIGURE 4

Differenced range as an angle measurement.

2.3.3.1 Very long baseline interferometry (VLBI)

A new technique for angle measurement is being tested in the Voyager mission. This involves very long baseline interferometry (VLBI), a technique developed by radio astronomers [Cohen 1969]. A spacecraft signal modulated by a pure sinusoidal tone, or an on-board noise source is observed by two DSN stations with synchronized clocks. Accuracy of fractions of seconds of arc can be achieved in short times. The allied technique of ΔVLBI finds the spacecraft angular position with respect to cosmic radio sources. Accuracies of about 10^{-2} arc seconds should be available from VLBI in the 1980s, and ΔVLBI promises even greater accuracies [Anderson and Estabrook, 1979].

2.4 Command

The command link (Earth-to-space) is characterized by the need for extreme reliability (BER $\leq 10^{-5}$). Commands must get through despite pointing errors on the spacecraft, and weather effects on Earth. As a result, the link budget is established for almost omnidirectional receiving antennas on the spacecraft, and the command frequency is firmly established at S-band (in order to stay below the frequencies that become vulnerable to terrestrial weather effects). The data rate requirements for the command link are determined by the size of the onboard computers, which control the spacecraft.

Most onboard activities are preprogrammed into these computers by periodic command sequences. It is desirable to complete these transmissions within the view period of a single ground transmitter (about 8 hours). To have the capability of completely reloading the computer in this time, the command link operates at 16 bits per second in the case of Voyager [Edelson et al, 1979]. The command signal (S-band) will be the last to be impacted by plasma effects, but it will be impacted when, for example, the spacecraft passes behind the solar corona at which point it suffers more degradation than the X-band signal due to the greater plasma effects at the lower frequency.

A typical command signal consists of Manchester-coded data bits PSK modulated onto a square wave subcarrier. Manchester coding is used to provide bit synchronization. The command channel error rate follows curve 1 of Figure 3.

2.5 Noise Considerations

Natural noise at microwave frequencies is treated from the standpoint of emission noise in the Earth's atmosphere in CCIR Rep. 683 and Rep. 720. Noise temperature in deep space receiving equipment (including antenna losses) is treated in Rep. 536-1. System noise temperature for Earth stations at S-band runs about 22.3K (see Table I), which at X-band rises to about 28.5K. These extraordinarily low temperatures make the deep-space system particularly vulnerable to gaseous or plasma emission noise.

3. SUMMARY

The telecommunications signal in deep-space missions serves a number of distinct purposes. Each of these uses has its own criteria for what constitutes significant signal degradation. Examples for the Voyager mission follow.

Uplink

The command signal increases its bit-error-rate (BER) a factor of 10 with a 1.1 dB decrease in signal-to-noise ratio.

Downlink

Radio science celestial mechanics experiments need to determine range to decimeters, and hopefully, centimeters at planetary distances.

The information transmitted by the telemetry signal is degraded by a factor of 10 in BER by a 0.2 dB decrease in SNR for the non-imaging data and by 0.7 dB decrease in SNR in the imaging data.

The navigation determinations currently rely on a minimum of 3 meter accuracy in the doppler and ranging determinations and anticipate further accuracies of less than 1 meter.

The estimated effects of ionization in the solar corona and solar wind for a spacecraft on the other side of the Sun, whose propagation path comes within four solar radii (4 $R_\odot$) of the center of the Sun, are tabulated in Table III. It is clear that several effects have become of significant magnitude. Also note that not all the effects are inversely dependent on the frequency of the source. Those due to scattering can be significantly shallower in their decrease with increasing carrier frequency.

TABLE III

Magnitude, critical threshold and frequency dependence at S-band of the various propagation effects for a propagation path traversing the solar corona to a closest approach of $4R_\odot$ of the Sun. One way traversal.

Effect	Magnitude (at 2.3 GHz, $4R_\odot$)	Critical Threshold	Frequency Dependence (f) (see Section II)
Faraday Rotation	20-200° (3-7° in ionosphere)	0.5° (see note 1)	$1/f^2$
Group Delay	17 μsec (250 nsec in ionosphere)	20 ns (see note 2)	$1/f^2$
Angular Broadening	0.02-2 min arc	±2 min of arc (see note 3)	$1/f^{2.2}$ to $1/f^3$
Spectral Broadening	7-16 Hz	0.2 Hz (see note 4)	$1/f^{1.2}$ to $1/f^2$
Absorption	negligible	0.1 dB	$1/f^2$
Dispersion	10 nsec/MHz	2 ns/MHz (see note 5)	$1/f^3$
Intensity Scintillation	saturates (m = 1)	m = 0.0024 (see note 6)	$1/f^{1.42}$ to $1/f^{1.2}$
Phase Scintillation	(see 3.1 of Section II)	±4° (see note 7)	$1/f^1$

Notes:

1. Telecommunication signals are normally circularly polarized. Faraday rotation is used as a sensing tool for studying the solar corona. Measurement accuracy is to be better than 0.5° for effective system time constants 30-100s [Volland et al, 1977].

2. An accuracy of 3 m in range requires an accuracy of 20 ns in group delay. This is achieved in practice through careful combination of several techniques and correction for plasma effects [Melbourne 1976].

3. This value (2 min of arc) is for the 64 m antenna at S-band and represents 0.1 dB decrease in signal level if the energy is spread uniformly over a ±2' cone of angles. At X-band the corresponding value is ±5 min of arc.

Notes (continued)

4. The value of 0.2 Hz is a lower limit on reported spectral broadening (Helios 1975 as reported in Woo 1978). In principle spectral broadening by a few tens of Hertz could cause the phase lock loop to lose lock but in practice this is unlikely.

5. At present a 10 MHz band is available for ranging. A value of 2 nanoseconds per megahertz corresponds to a difference in group delay of 20 nanoseconds across this band which in turn corresponds to a 3 meter ranging error.

6. A variation in power of $\pm$2.4% equates to $\pm$0.1 dB. The scintillation index is defined as the RMS fluctuations of intensity about the mean, relative to the mean. The $\pm$2.4% has been equated to this RMS fluctuation.

7. Phase is accumulated with an accuracy of 4° by the Doppler-cycle counter in the range-change navigation system [Melbourne, 1976]. A more serious effect has to do with the ability of the phase lock loop to track rapid phase excursions.

SECTION II

THEORY AND OBSERVATION OF PROPAGATION IN EXTRATERRESTRIAL PLASMAS

1. INTRODUCTION

Plasmas occur in various forms and it is necessary to specify several parameters to determine the regime of the plasma. These parameters are temperature, magnetic field, degree of ionization, electron density, and homogeneity. The effect of the plasma in each regime on an electromagnetic wave passing through it will depend on the frequency of the wave relative to the local plasma frequency and the gyrofrequencies of the charged particles, the angle of the direction of propagation relative to the magnetic field (if any), and the polarization of the wave. A description of radio waves in plasmas is found in Report 222-4, and fuller descriptions may be found in Ginzburg [1967], Stix [1962], Shkarofsky et al. [1966], Wait [1968] and Yeh and Liu [1972].

The distinction between a warm and cold plasma is whether the wavelength in the plasma is much greater than (cold) or much less than (warm) the Debye length, λ_D.

$$\lambda_D = 69 \left(\frac{T}{N}\right)^{1/2} \text{ meters}$$

where T is the temperature in kelvin and N is the electron density (m^{-3}). In the Earth's ionosphere, the Debye length is typically 0.3 cm in the daytime and 1 cm at night, and the plasma may be considered cold at S- and X- (but not K-) band. In the solar corona, the Debye length is typically 0.1 to 1 meter, and the plasma appears lukewarm to the 13-cm waves used at S-band for deep-space telecommunications, and warm for X-band and above.

The critical magnetic field, B_c (that is, the level at which a plasma ceases to behave isotropically), may be taken as the field strength, H, at which the energy in the magnetic field ($1/2\ \mu_o H^2$) is equal to the thermal energy of the electrons ($3/2\ N\ k\ T$). Hence,

$$B_c = \sqrt{3\ \mu_o\ N\ k\ T} = 7.21 \times 10^{-11}\ \sqrt{NT} \text{ gauss}$$

where k is Boltzmann's const. (1.38×10^{-23} J/K) and μ_o is the free-space permeability.

In the Earth's ionosphere, B_c is typically 2 to 3×10^{-3} gauss, whereas the Earth's magnetic field at ionospheric heights is 0.3 to 0.6 gauss. Hence, the Earth's ionosphere is strongly magnetically controlled. In the solar corona, B_c is $\sim 10^{-2}$ gauss at 4 solar radii from the Sun's center ($4R_\odot$) and the static magnetic field is $\sim 10^{-1}$ gauss, so magnetic control is still the rule. Illustrated in Figure 5 are the plasma domains traversed by a radio signal from a spacecraft near solar conjunction received at the Earth's surface (see Figure 6). We see that the 2.3 GHz signal is largely in the "warm-anisotropic plasma" domain until it passes into the "cold-anisotropic" domain (i.e., the Earth's ionosphere). This change of domains indicates caution in use of the cold plasma theory. Fortunately, the warm

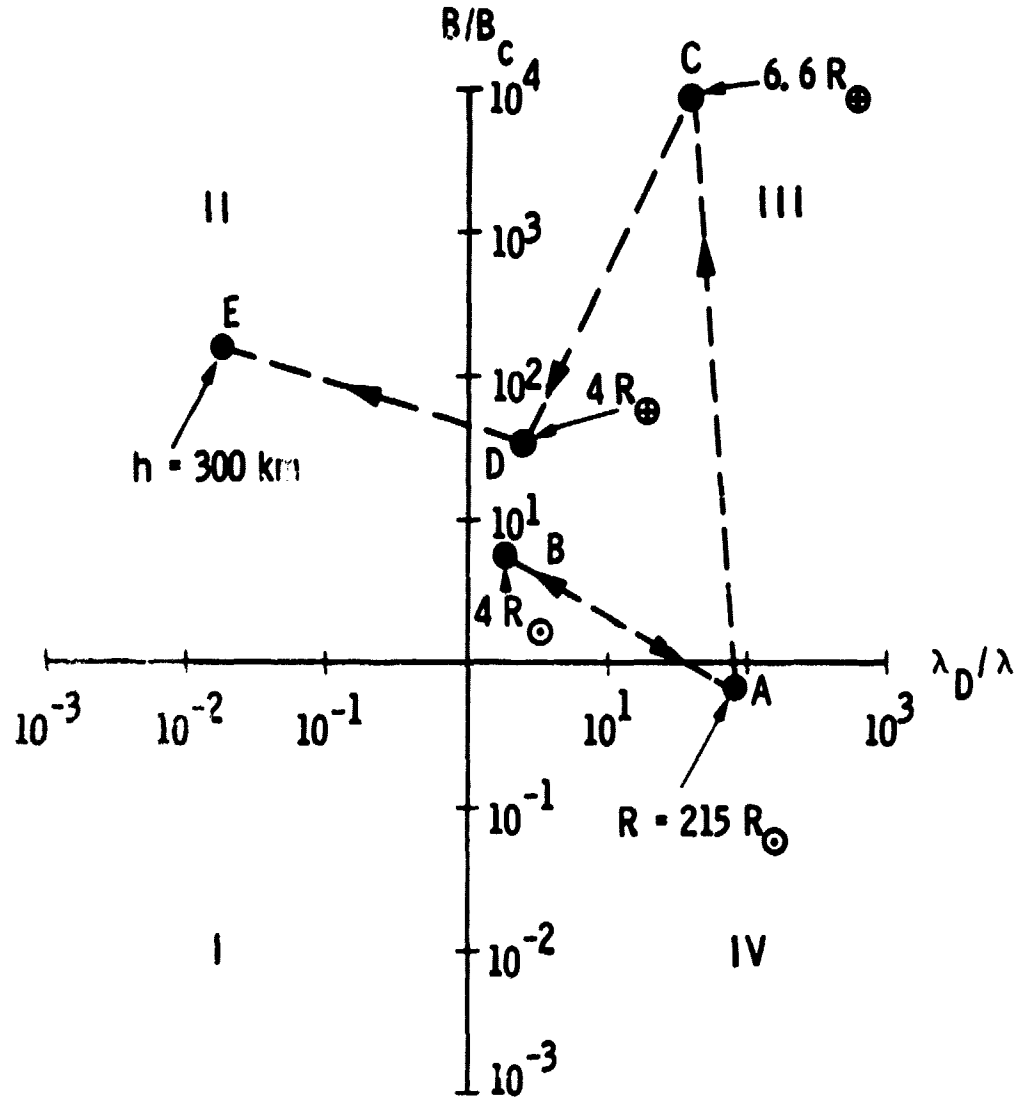

FIGURE 5

Plasma domains traversed by 2.3 GHz spacecraft signal. Points A through E are specified in Table IV. Spacecraft located as shown in Figure 6. Domains are determined by the Debye shielding distance λ_D and the magnetic critical value B_c (see text) and are: I - cold isotropic, II - cold anisotropic, III - warm anisotropic, and IV - warm isotropic. Plotted points are those marked on Figure 6: A - spacecraft location, B - solar corona (4 $R_\odot$), C - Earths' ionosphere (300 km), D - plasmasphere (4 $R_\oplus$), E - geostationary orbit (6.6 $R_\oplus$).

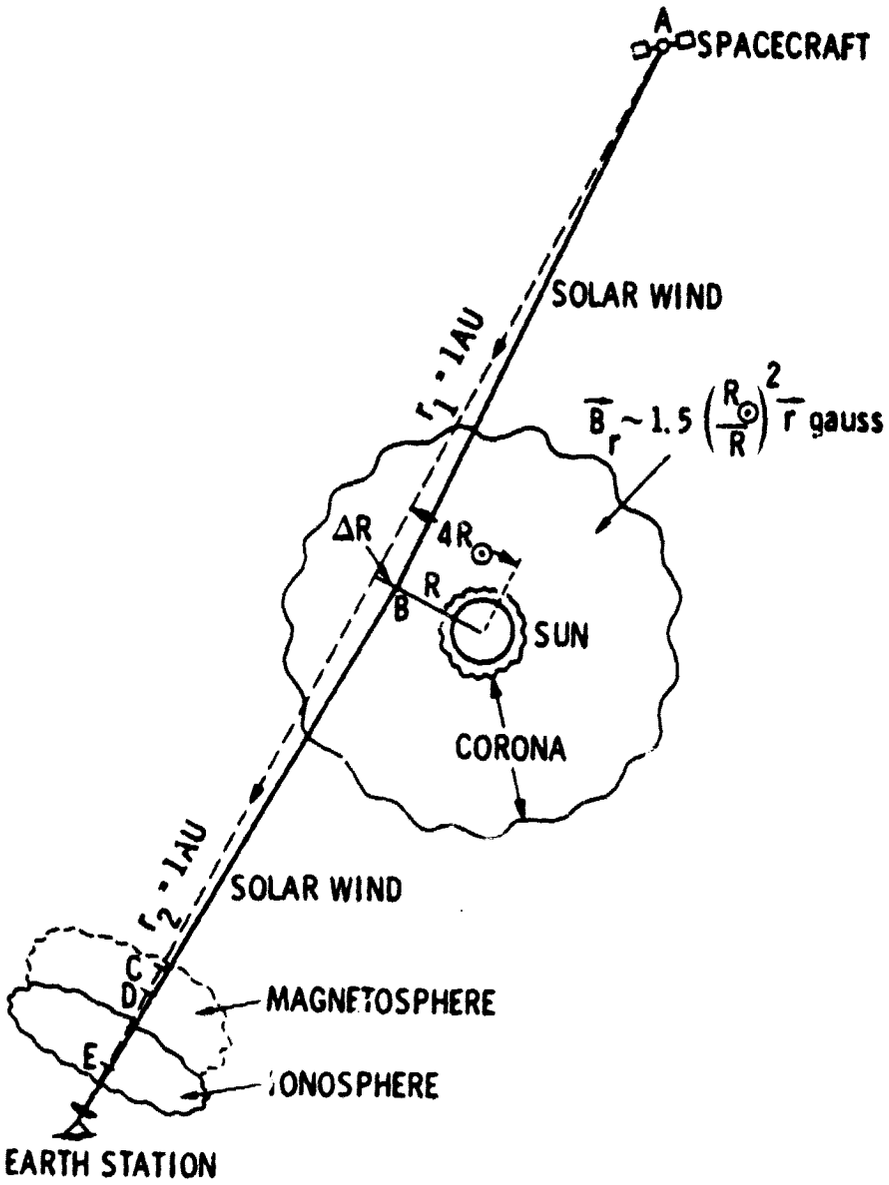

FIGURE 6

Propagation path used for sample calculations. Spacecraft is at A, closest approach to Sun is at B, peak of Earth's ionosphere is at E. Also shown are points D, just within the plasmapause, and C, the geostationary distance.

vs. cold plasma distinction becomes important when the wave velocity of the signal becomes comparable to the particle velocities in the medium [Yeh and Liu, 1972], and that is not the case for any of the microwave links under consideration.

The effect of magnetic control will be dealt with as the need arises in the topics treated below.

In the discussion that follows the following homogeneous plasma effects on radio waves are treated first: group delay, absorption, dispersion, Faraday rotation and Doppler shift. This is followed by a discussion of effects due to inhomogeneities, including phase scintillations, intensity scintillations, spectral and angular broadening, and coherence bandwidth.

The propagation path used as an example in the following discussions is shown in Figure 6. It is the same one used in connection with Table III in the main body of this report. Table IV contains a listing of the various parameters used in the text for three locations, which are marked on Figure 6. An objective of Table IV and the discussion to follow is to illustrate circumstances where it is safe to use simple approximations.

2. MICROWAVE PROPAGATION IN A HOMOGENEOUS ANISOTROPIC PLASMA

The Appleton-Hartree equation for the complex refraction index in a homogeneous anisotropic ionized medium is given by

$$n^2 = 1 - \frac{X}{1 - iZ - \left[\frac{1}{2} Y_T^2/(1 - X - iZ)\right] \pm \sqrt{\left[Y_T^4/4(1 - X - iZ)^2\right] + Y_L^2}} \qquad (2)$$

where the nomenclature is that given by Ratcliffe [1959]:

- e,m charge and mass of the electron
- θ Angle between the direction of phase propagation and the external magnetic field $\vec{B}_o$.
- ν Collision frequency between electrons and other particles.
- ω_N^2 The square of the angular plasma frequency of the medium ($Ne^2/\varepsilon_o m$), where N is the electron density, and ε_o is the permittivity of free space.
- f_N Plasma frequency ($\omega_N/2\pi$).
- ω_H Angular gyrofrequency or cyclotron frequency of the electrons ($|e|\ \vec{B}_o/m$).
- ω Angular frequency of the wave
- X $(\omega_N/\omega)^2$.
- $\vec{Y}$ $[e/(m\omega)]\vec{B}_o$.
- Y ω_H/ω.
- Y_L $Y \cos\theta$
- Y_T $Y \sin\theta$

Table IV. Characteristics of the Plasma State Pertinent to 2.3 GHz Transmission

Item	Parameter	Units	(a) Deep Space Location (Extraterrestrial)		(b) Near-Earth Space Location (Terrestrial)		
			A	B	C	D	E
			Interplanetary Space 1 AU from the Sun	Solar Corona 4 $R_\odot$ from Sun's Center	Magnetosphere 1 6.6 $R_\oplus$ (Geostationary Orbit)	Magnetosphere 2 4 $R_\oplus$ (inside plasmapause)	Ionosphere 300 km Altitude
1.	Electron density, N	m^{-3}	7.5×10^{6}	1.2×10^{11}	3×10^{7}	3×10^{8}	10^{12}
2.	Effective temperature, T	K	1.5×10^{5}	1.5×10^{6}	5300	10^{4}	1200
3.	Flow speed, v	Km/s	450.	72.	--	--	--
4.	Magnetic field, B_o	gauss	5×10^{-5}	0.14	10^{-3}	5×10^{-3}	0.4
5.	Collision frequency, ν	s^{-1}	1.2×10^{-5}	5.9×10^{-3}	2.3×10^{-3}	5.9×10^{-2}	1100
6.	Plasma frequency, f_N	Hz	2.5×10^{4}	3.1×10^{6}	4.9×10^{4}	1.6×10^{5}	9×10^{6}
7.	Electron gyrofrequency, f_H	Hz	140	3.9×10^{5}	2.8×10^{3}	1.4×10^{4}	1.1×10^{6}
8.	$X = (\omega_N/\omega)^2$		2.9×10^{-12}	1.8×10^{-6}	4.5×10^{-10}	4.8×10^{-9}	1.5×10^{-5}
9.	$Y = \omega_H/\omega$		6.1×10^{-8}	1.7×10^{-4}	1.2×10^{-6}	6.1×10^{-6}	4.9×10^{-4}
10.	$Z = \nu/\omega$		8.5×10^{-16}	4.1×10^{-13}	1.6×10^{-13}	4.1×10^{-12}	7.9×10^{-8}
11.	$n_o = (1 - X)^{1/2}$		$1 - 1.4 \times 10^{-12}$	$1 - 9.2 \times 10^{-7}$	$1 - 22 \times 10^{-10}$	$1 - 2.4 \times 10^{-9}$	$1 - 7.7 \times 10^{-6}$
12.	$n_{QL} = [1 - X/(1-Z-Y)]^{1/2}$		$1 - 1.4 \times 10^{-12} + [8.8 \times 10^{-20}]$	$1 - 9.2 \times 10^{-7} + [1.6 \times 10^{-10}]$	$1 - 2.2 \times 10^{-10} + [2.7 \times 10^{-16}]$	$1 - 2.4 \times 10^{-9} + [1.5 \times 10^{-14}]$	$1 - 7.7 \times 10^{-6} + [7.5 \times 10^{-9}]$
13.	$n_g = 1/n_o$		$1 + 1.4 \times 10^{-12}$	$1 + 9.2 \times 10^{-7}$	$1 + 2.2 \times 10^{-10}$	$1 + 2.4 \times 10^{-9}$	$1 + 7.7 \times 10^{-6}$
14.	$n_g n_{QL}$		$1 + 8.8 \times 10^{-20}$	$1 + 1.6 \times 10^{-10}$	$1 + 2.7 \times 10^{-16}$	$1 + 1.5 \times 10^{-14}$	$1 + 7.5 \times 10^{-9}$
15.	Debye length, λ_D	m	9.8	0.24	21.8	0.40	2.4×10^{-3}
16.	Plasma state, λ_D/λ		75 (warm)	1.8 (lukewarm)	168 (warm)	3.1 (lukewarm)	1.8×10^{-2} (cold)
17.	Critical magnetic field, B_c	gauss	7.6×10^{-5}	3.1×10^{-2}	2.3×10^{-5}	1.25×10^{-4}	2.5×10^{-3}
18.	Magnetic control, B/B_c		0.66 (weak)	4.6 (moderate)	43.5 (strong)	40 (strong)	160 (very strong)

Z ν/ω

R Wave polarization

The implications of this equation (for a cold plasma) and the associated theory can be found in many excellent texts, for example, Ratcliffe [1959], Budden [1961] and Davies [1968]. Its limitations and extensions may be found Wait [1968] in Yeh and Liu [1972] and Booker [1975].

Longitudinal propagation ($\theta = 0°$) and transverse propagation ($\theta = 90°$) offer significant simplifications, and have been worked out in detail. The quasi-longitudinal or Q.L. approximation [Booker, 1934] is possible when

$$| Y_T^2/2Y_L | << | 1 - X - iZ | \tag{3}$$

This leads to the Q.L. approximation of (1):

$$n^2 = 1 - \frac{X}{1 - iZ \mp Y_L}, \qquad R = \mp i \tag{4}$$

where two counterrotating circularly polarized waves are allowed. As the left side of (3) varies as f_H/f (and f_H, the electron gyrofrequency, is normally 1 MHz or less), and the right side of (3) approaches unity with increasing frequency, it is clear that for frequencies above 1 GHz, the quasi-longitudinal approximation is good except for a small fraction of a degree around $\theta = 90°$. In the discussion that follows, the Q.L. approximation will be assumed to be valid.

2.1 Group Delay

Group delay is discussed in Section 4.2 of CCIR Report 263-4 (and in the texts referred to above) for the isotropic collision-free case. It is instructive to examine the radio science and navigation needs in deep-space research to see if that discussion will suffice.

The group refractive index n_g may be defined in terms of the phase refractive index n

$$n_g = \frac{d}{d\omega}(n\omega) = n + \omega \frac{dn}{d\omega} \tag{5}$$

This expression is evaluated for the collisionless case in Davies [1968], and for the complete Appleton-Hartree expression (2) in Budden [1961].

If the Q.L. approximation (4) for the phase refractive index is reduced to the collisionless isotropic case ($n^2 = 1 - X$), then from (5)

$$n_g = \frac{d}{d\omega}(n\omega) = \frac{1}{n} \qquad \text{(isotropic collisionless case)} \tag{6}$$

which is a familiar case in which $nn_g = 1$. However, retention of the O.L. approximation by substituting (4) in (6) and performing the differentiation in (6) gives

$$n_g = \frac{1}{n}\left\{1 + \frac{X(Z + Y)}{2(1 - Z - Y)^2}\right\} \qquad \text{(Q.L. approximation with collisions)} \tag{7}$$

Expression (6) is shown numerically in line 13 and expression (7) is evaluated in line 14 of Table IV. The difference between the isotropic value of the refractive index, n_o, and that using the Q.L. approximation is seen to be negligible, as is the error in computing n_g, the group refractive index, as 1/n (the reciprocal of the phase refractive index as in (6)). Hence, for purposes of computing group delay, the approach used in Report 263-4 is still valid for deep-space problems.

The time delay, T (in seconds), of a radio signal traversing the deep-space-to-Earth path L (spacecraft to Earth station, shown in Figure 6) is given from (6) by

$$T = T_o + \Delta T = \frac{1}{c}\int_L n_g\, d\ell = \frac{1}{c}\int_L \left(1 + \frac{40.31}{f^2} N\right) d\ell = T_o + \frac{40.31}{cf^2}\int_L N\, d\ell \tag{8}$$

where N is electron density in m^{-3}, and f is the frequency in Hertz which leads to:

$$\Delta T = \frac{1.3446 \times 10^{-7}}{f^2}\int_L N\, d\ell \tag{9}$$

where ΔT is the group delay due to the presence of free electrons measured in seconds. It is a function only of the integrated electron density along the propagation path and the radio-wave frequency.

As seen in Figure 7, the excess time delay for an S-band uplink and X-band downlink reached 12 μs. Assuming identical propagation paths, the delay on the downlink (8.4 GHz) would be 7.33% that of the S-band (2.3 GHz) uplink. Thus, 11.2 μs can be attributed to the S-band uplink. From (9) we have

$$\text{TEC} = \int_L N\, d\ell = 7.493 \times 10^6 \Delta T\, f^2 \text{ el m}^{-2} \tag{10}$$

$$= 4.44 \times 10^4 \text{ hexem}$$

where TEC stands for total electron content, and the hexem is a unit of content defined as 1 hexem = 10^{16} electrons/meter^2.

The simple approximations of (6) through (10) will suffice for all conceivable microwave applications.

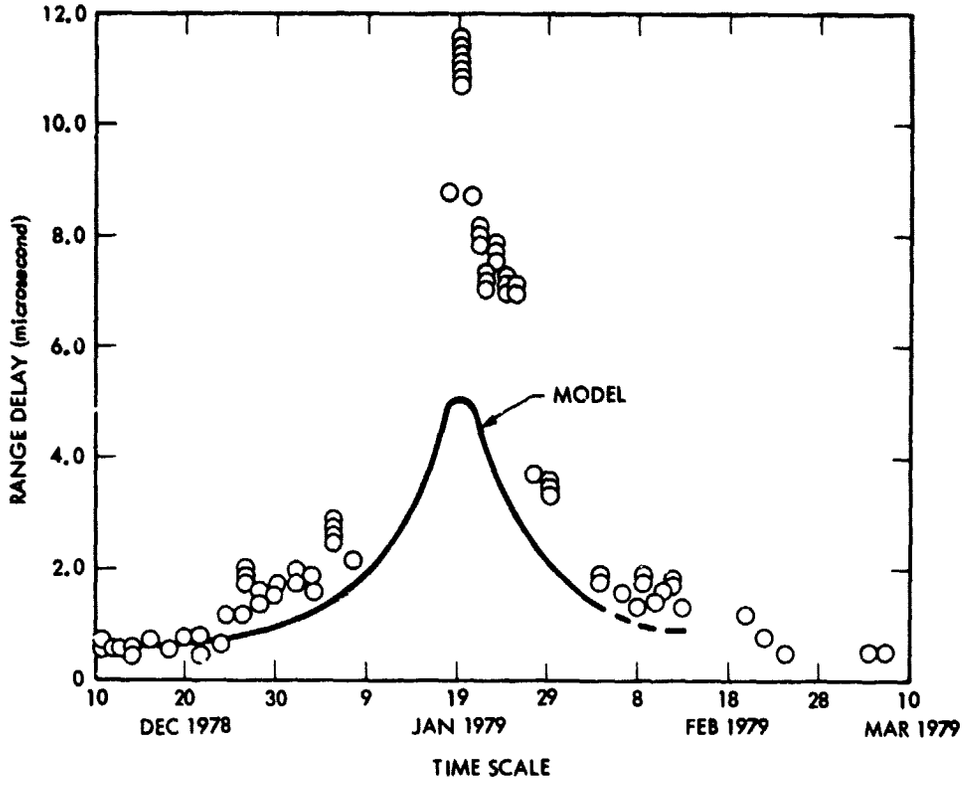

FIGURE 7

Range delay experienced by Viking spacecraft during January 1979 solar conjunction for S-band uplink and X-band downlink. Elongation is 1.02° over southern heliographic pole ($R \sim 4\ R_{\odot}$ per figure 6). Model based on 1976 Viking solar conjunction. (Courtesy J. C. Breidenthal and T. A. Komarek, JPL).

2.2 Dispersion

A dispersive medium is one in which the refractive index (n) is a function of frequency (or free-space wavelength). In a plasma where $\omega >> \omega_N$, and $\omega >> \omega_H$, the dispersion is said to be normal if the phase refractive index is an increasing function of frequency. Differentiating (9) yields a particularly useful relation (assuming the path does not change):

$$\frac{dT}{df} = \frac{2.689 \times 10^{-7}}{f^3} \int_L N \, d\ell \quad \text{seconds/Hz} \tag{11}$$

For example, using the TEC value derived in (10), we find $dT/df = 9.813 \times 10^{-15}$ s/Hz or 9.813 nanoseconds/MHz for the difference in delay time for components of the signal spaced one megahertz apart in our example (approximately the configuration of Figure 6).

2.3 Absorption

It is known that a negligible role is played by plasma absorption in microwave propagation through the solar corona and interplanetary medium, but it is worth reviewing why absorption is negligible. The path absorption, L_a, is given [Davies, 1968] as:

$$L_a = \int_s A \, ds \quad \text{decibels} \tag{12}$$

where

$$A = 1.15 \times 10^{-3} \, N\nu f^{-2} \quad \text{decibels/km} \tag{13}$$

s is distance in km, N is electron density in m^{-3}, ν is the pertinent collision frequency, and f is the radio wave frequency in Hertz. The pertinent collision frequency turns out to be for coulomb collisions of electrons with ions [Rishbeth and Garriott, 1969]:

$$\nu_{ei} = \left\{59 + 4.18 \log_{10}(T^3/N)\right\} 10^{-6} \, NT^{-3/2} \quad \text{seconds}^{-1} \tag{14}$$

Here the important point is that ν_{ei} depends on $T^{-3/2}$. In other words, the collision frequency decreases with increasing temperature. As a consequence, at point B of Table IV (the closest approach to the Sun for the propagation path of Figure 6), the absorption coefficient from (13) at 2.3 GHz is only:

$$A = 3.2 \times 10^{-11} \text{ decibels/km}$$

If this absorption coefficient were to obtain for the entire propagation path of two astronomical units (300 million kilometers), the path absorption, L_a, would amount to only 0.01 dB. Alternatively, if the absorption coefficient were to increase by a factor of one thousand (to 2.5×10^{13} m^{-3}) as would be appropriate to 1.4 solar radii rom the center of the Sun, and if this absorption coefficient were to hold for 300,000 km, the path absorption would still only amount to 0.01 dB. Clearly, absorption at microwaves is negligible for the solar corona and solar wind.

2.4 Faraday Rotation

The two slightly different refractive indices given by (3) for the quasi-longitudinal approximation indicate that a linearly polarized wave may be treated as two counterrotating circularly-polarized waves with slightly differing phase velocities. For microwave frequencies, the binomial expansion may be used on (3):

$$n = \sqrt{1 - X/(1 \pm Y_L)} \cong 1 - 1/2\ X(1 + Y_L)$$

which leads to the Faraday rotation formula for rate of change of the angle of rotation of the plane of polarization with distance:

$$\frac{d\Omega}{ds} = \frac{\pi}{\lambda} X\ Y_L = 1.3548 \times 10^{-10}\ N\ B_L \quad \text{deg/m} \tag{15}$$

where N is electron density (m^{-3}), and B_L is the longitudinal component of the magnetic field in gauss. Good discussions of Faraday rotation measurements to determine total electron content in the Earth's ionosphere are found in Garriott, et al. [1970] and Budden [1961].

Faraday rotation measurements of radio paths through the solar corona are treated by Levy et al. [1969], Stelzried et al. [1970] and Volland et al. [1977].

The magnetic field emanating from the sun is roughly radial at distances greater than about 2 solar radii with a spiral effect dominating at longer distances. Parker [1963] has approximated the angle of the spiraling lines by

$$\tan \alpha = \frac{r\Omega_s}{v} \tag{16}$$

where r = distance from center of the sun, km
Ω_s = Sun rotation rate, rad. sec^{-1}
v = velocity of the solar wind, km sec^{-1}

As a consequence the magnetic field is about 1.7° off radial at $4R_\odot$ for the parameters given for location B in Table IV and about 46° off radial at 1AU for the parameters for location C, so there is a slight asymmetry to the magnetic field as encountered by a radio wave following a path such as illustrated in Figure 6. If the solar magnetic field were perfectly radial (and maintained the same polarity) and the electron density spherically

symmetric, Faraday rotation would accumulate (wind up) in one sense of rotation up to point B of Figure 6 and then unwind by an identical angle and no rotation would be observed on Earth. This, however, is not the case as illustrated for Helios in Figure 8. Actually the magnetic field will have segments of constant polarity with neighboring regions of opposite polarity thus greatly increasing the chances for non-cancellation of integrated Faraday rotation. Observed Faraday rotation for solar conjunction of spacecraft has been analyzed and found to be in good agreement with current understanding of magnetic sectors in the corona and solar wind [Volland et al., 1977].

2.5 Doppler Shift

The Doppler shift, Δf, of a signal transmitted with a frequency, f, from a moving spacecraft (Figure 6) is given by

$$\Delta f = \frac{f}{c}\frac{dP}{dt} = -\frac{f}{c}\frac{d}{dt}\int_T^R n\, ds \qquad (17)$$

where P is the phase path from transmitter to receiver and n is the phase refractive index. As indicated in lines 11 and 12 of Table IV, the difference between the isotropic and Q.L. approximation is negligible, and the phase refractive index n may be approximated by $n \simeq 1 - X/2$ just as can the group index $n_g \simeq 1 + X/2$. As range change is acquired in tracking both from integrating the Doppler observations ($D\phi$) and differencing group path measurements (D_g), the difference ($D_g - D\phi$) is a measure of change in integrated electron content along the ray path [Callahan, 1975]. This differenced range versus integrated doppler (DRVID) is used by NASA to provide one measure of the change in total electron content (TEC) along the propagation path. The phase path data utilized in DRVID are also the source of much of the data for the fluctuation studies discussed in the next section.

3. MICROWAVE PROPAGATION IN INHOMOGENEOUS INTERPLANETARY PLASMA

Interplanetary scintillations (IPS) have been studied using natural stellar sources since the discovery of IPS [Hewish, et al., 1964]. The observing frequencies are commonly in the VHF and UHF band [Coles, et al., 1974], but there are compensating advantages to using spacecraft signals. For example, in addition to the study of intensity scintillations, one may observe spectral broadening and phase scintillations if one has access to coherent monochromatic spacecraft signals. This adds considerably to the range of scale sizes of the medium that can be studied as shown in Figure 9 [Woo, 1977]. The plot is in terms of the spatial wave number, K, which is related to the scale size ℓ by $K = 2\pi/\ell$. Hence it can be seen that intensity scintillations are limited in applicability to the study of scale sizes from 60 m to 600 km, whereas phase scintillations extend from 1 km to several AU.

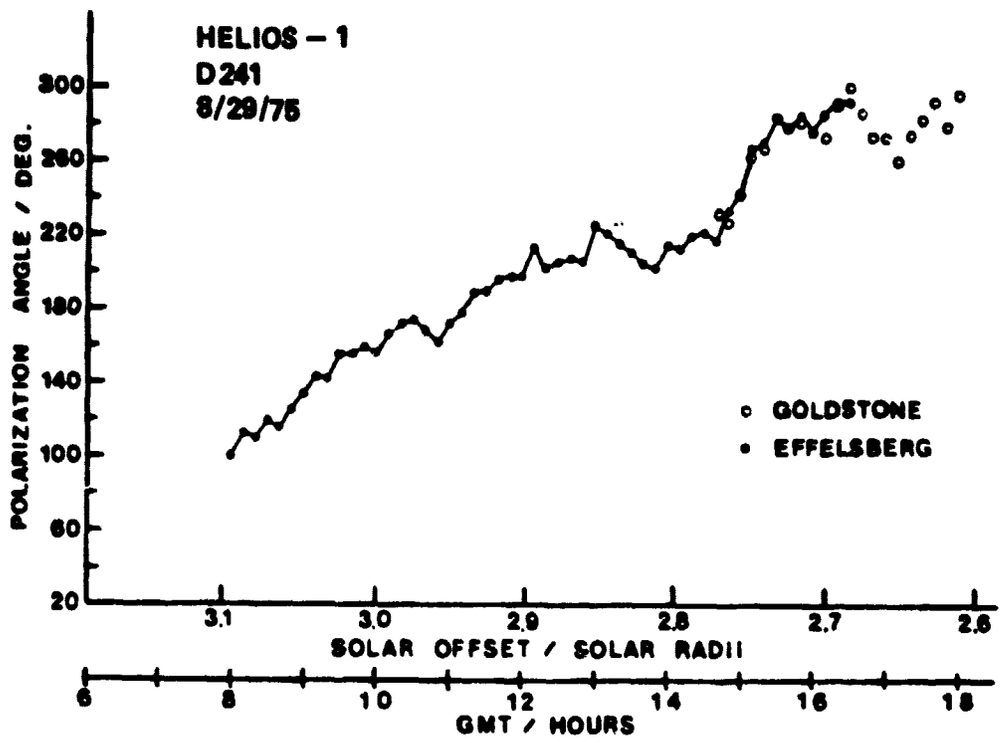

FIGURE 8

Polarization angle (coronal Faraday rotation) measured on day number 241 of 1975 during the second of two Helios-1 occultations. Recording stations are Goldstone, California and Effelsberg near Bonn, F.R.G. (after Volland et. al. 1977).

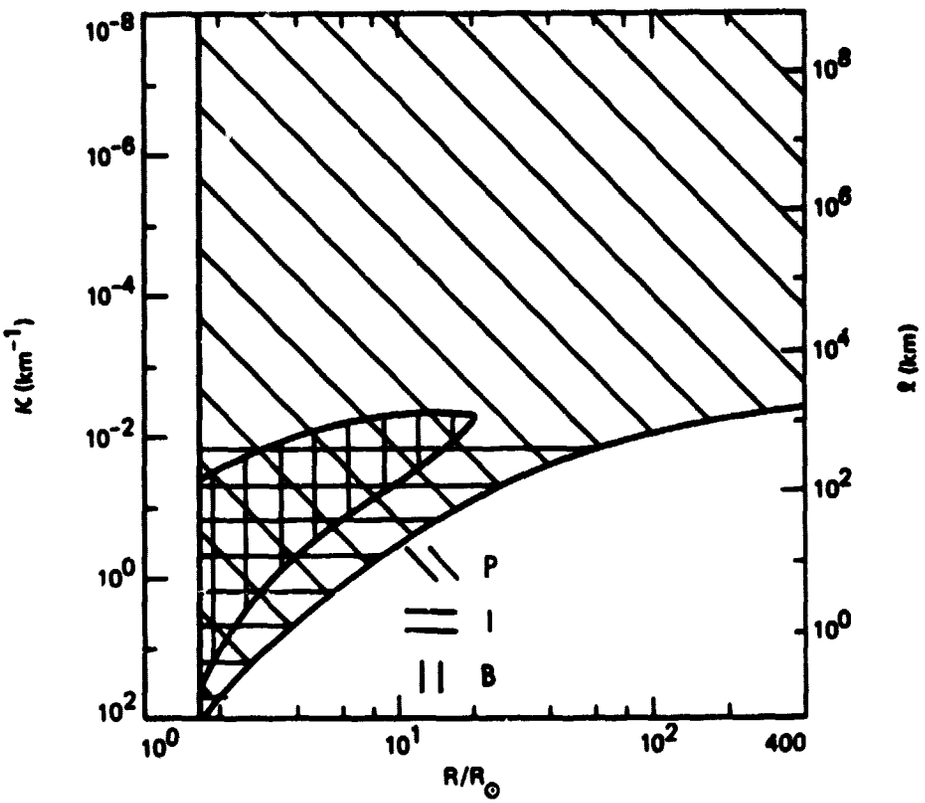

FIGURE 9

Range of heliocentric distances and spatial wavenumbers, K (related to the scale size ℓ by K = $2\pi/\ell$) for spacecraft radio scattering observations for 2.3 GHz signal and SNR of 40 dB. P = phase scintillations, I = intensity scintillations, B = spectral broadening (after Woo, 1977).

All aspects of scintillation become critical as the propagation path passes near the Sun and these will be considered in turn.

3.1 Phase Scintillations

Phase scintillations of spacecraft signals have been used to study the solar wind and solar corona because they contain information on a wide range of scale sizes [Woo, et al., 1976a,b; Woo, 1977; Woo and Armstrong, 1979]. Extensive phase difference scintillation observations (2700 hours) have been made simultaneously at 2.3 and 8.4 GHz in 1976-1978 for heliocentric distance ranges, R, of 2-215 $R_\odot$. (The symbol $R_\odot$ stands for the solar radius, a distance of 696,000 km, and 215 $R_\odot$ is 1 AU, while R is the closest approach to the Sun of the propagation path and is sometimes called the impact parameter.)

The 8.4-GHz signal is phase coherent and exactly 11/3 the frequency of the 2.3-GHz signal. Hence by recording the phases $\phi_1 - 3/11\ \phi_2$, where ϕ_1 and ϕ_2 are the phases for 2.3 GHz and 8.4 GHz respectively, the effect of phase change on the uplink signal is cancelled out. An example of this phase difference measurement is shown in Figure 10 exhibiting both small-scale (minutes) and large-scale (hours) variations.

The phase difference spectra $W_{\phi d}(f)$ are computed by Fourier transforming the time series, squaring, and smoothing the result [Woo, 1975; Woo, et al., 1976a]. The resulting spectrum is shown in Figure 11.

The orbiters of the Viking Mission to Mars were equipped with S- and X-band dual-frequency (2.3 and 8.4 GHz) coherent radio systems [Michael, et al., 1977]. Spectra for various elongations (Sun center-Earth Station-spacecraft angles), ε (one solar radius corresponds to an elongation of about 0.27 degrees), are shown in Figure 12 [Woo and Armstrong, 1979]. The high frequency instrumental phase noise is white and is about 10^{-2} rad^2/Hz for the closed-loop spectra (inner three) of Figure 10 but is about 10^{-4} rad^2/Hz for the open-loop spectra (outer three) where it had become necessary to open up the receiver bandwidth due to spectral broadening.

A frequency spectrum of electron density, made up of in situ measurements made by a spacecraft as it moves along its orbit, is a one-dimensional wave number spectrum, V_{ne}; and Woo, et al. [1976b], have shown that if the three-dimensional wave number spectrum Φ_{ne} of the electron density fluctuations has a power-law dependence with spectral index p ($\Phi_{ne} \propto K^{-p}$ where K is the wave number), the frequency spectrum $W_{\phi d}$ of the phase-difference scintillations and the one-dimensional frequency spectrum V_{ne} (measured by in situ spacecraft) are both power-law with spectral indices p-1 and p-2 respectively. Specifically V_{ne} is related to $W_{\phi d}$ by

$$V_{ne}(f) = 4.39 \times 10^{27}\ W_{\phi d}(f)\ \frac{f_s}{v}\ \frac{K^2}{R}\ \frac{1}{(p-2)}\ \frac{\Gamma\left(\frac{p}{2}\right)}{\Gamma\left(\frac{p-1}{2}\right)} \qquad (18)$$

where $K = 2\pi/\lambda$ is the wave number, λ is the wavelength, R is the closest solar distance of the line-of-sight path in units of $R_\odot$, v is the solar wind velocity transverse to the line-of-sight path at R, f_s is the fluctuation frequency, c is the speed of light, Γ is the Gamma function, and all units are SI [Woo and Armstrong, 1979].

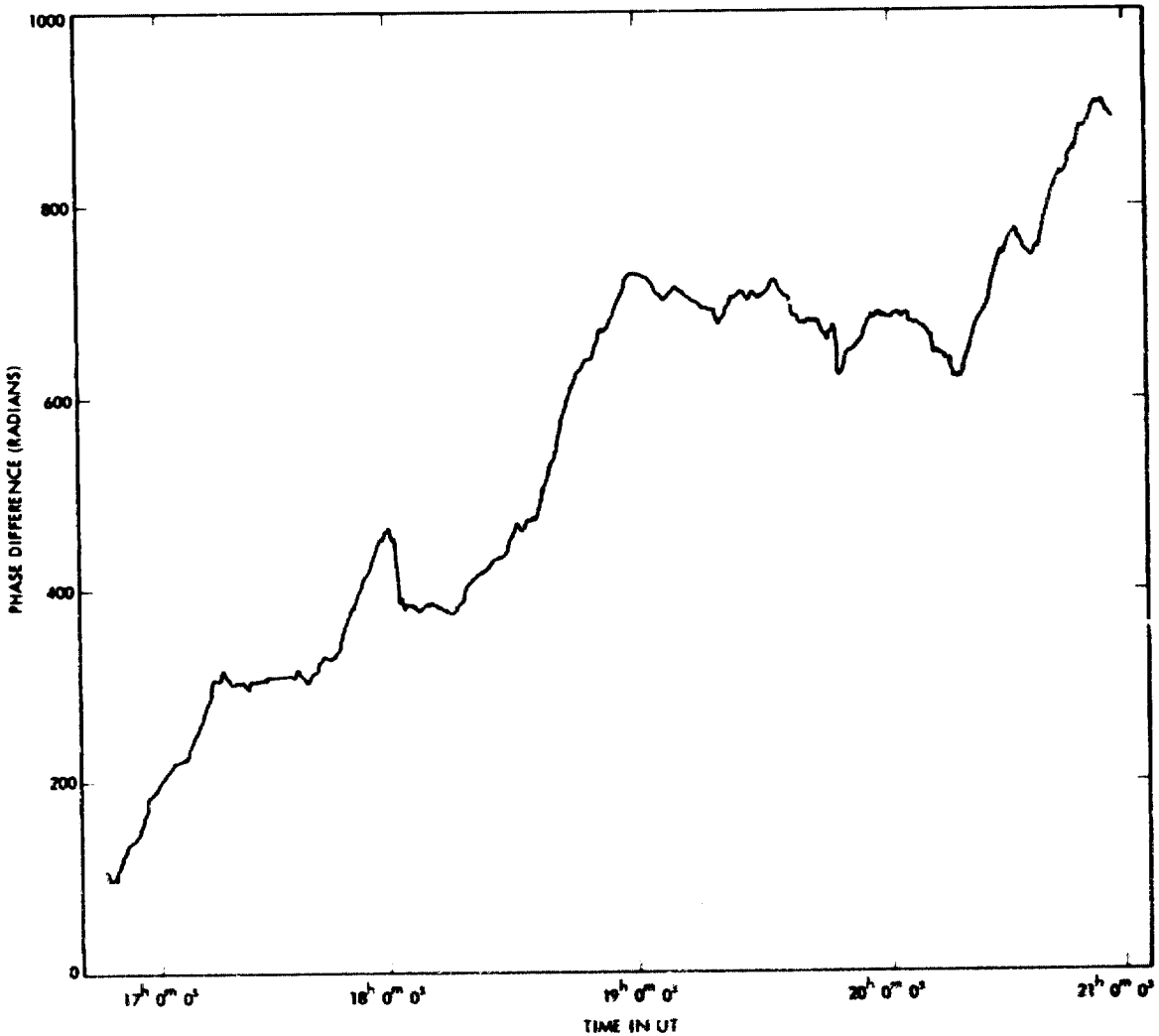

FIGURE 10

Time history in UT of Mariner 10 S/X phase difference in radians (arbitrary scale) taken on May 1, 1974 when the elongation angle was 11.5 degrees ($\sim$43 $R_\odot$). Phase difference data is discussed in the next. (After Woo et al. 1976b).

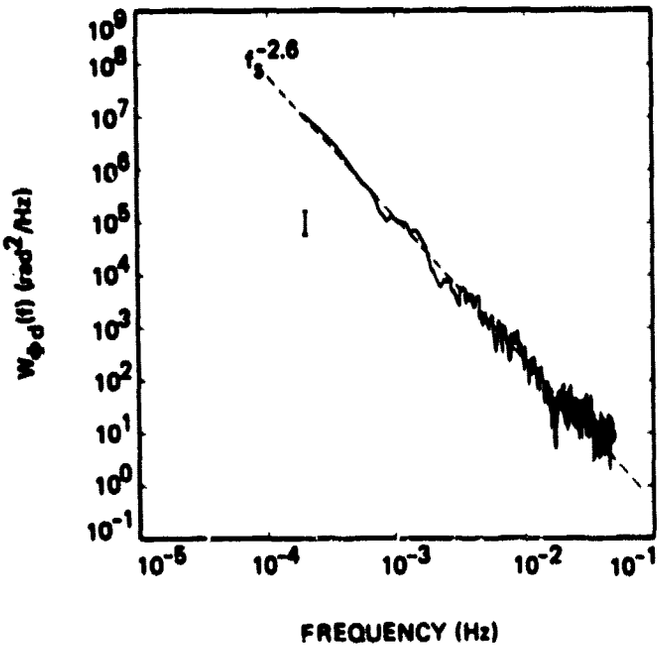

FIGURE 11

Frequency spectrum, Wϕd, for phase difference fluctuations shown in Figure 10. The dashed line represents the power law $f_s^{-2.6}$. The vertical bar defines the 90% confidence interval. The number of points used in the running point average m = 15 (after Woo et al. 1976b).

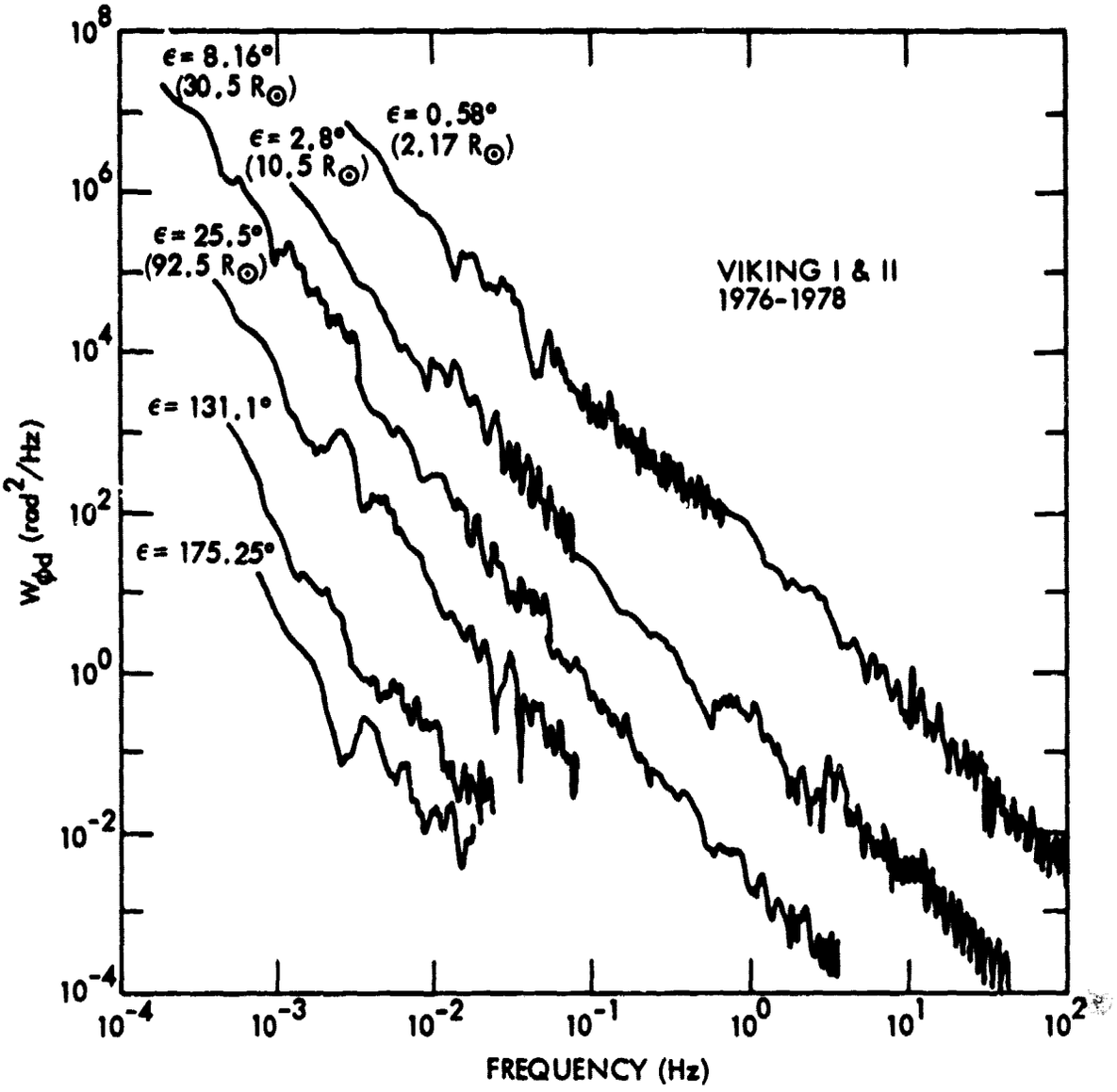

FIGURE 12

Typical power spectra, $W_{\phi d}$, of the Viking phase-difference scintillations observed over the entire solar elongation (E) range. The spectra for $R \leq 30.5\ R_\odot$ are of open-loop data while the rest are of closed-loop data (after Woo and Armstrong, 1979).

This relation, (18), based on the Rytov geometric-optics solution, applies for fluctuation frequencies less than the Fresnel frequency, which is the order of 1 Hz for weak scintillations when $R \geq 20\ R_\odot$. It allows the phase spectra of Figure 12 to be related to the spectra of electron density fluctuations. These are shown in Figure 13 for a large number of solar impact parameters. Note that the exponent of the fluctuation frequency exponent is now p-2 as compared to p-1 for the phase spectra of Figure 12. Hence the best fit to the spectra of Figure 12 is

$$W_{\phi d}(f) = 5.6\ f_s^{-2.65} R^{-2.45}\ \frac{\text{radians}^2}{\text{Hz}} \qquad (19)$$

where R is in solar radii ($20 \leq R \leq 100$) and f_s is in Hz.

3.2 Intensity Scintillations

Interplanetary scintillations (IPS) of natural sources beyond our solar system have been studied extensively from networks of observing sites on Earth's surface [Coles 1978, Coles and Harmon 1978]. The degree of scintillation is characterized by m, the scintillation index, defined as the rms fluctuation of intensity about the mean relative to the mean. Figure 14a shows how it varies with the strength of turbulence and wavelength, because turbulence increases as p decreases. Thus, m increases with turbulence if the turbulence is weak, reaching a maximum $m_{max} < 1$ at some P_{max}. Increasing turbulence beyond this point produces a sharp decrease in scintillation, which is due to the angular width of the source. The more nearly the source approximates a point source, the closer m_{max} approaches unity [Coles, Rickett and Rumsey, 1974]. Figure 14b illustrates the behavior of the scintillation m for a point source (Helios spacecraft) where it is seen that m becomes assymptotic to unity for $R < 10$ [Woo, 1979].

For spacecraft transmission, the behavior or extraterrestrial scintillation described in Report 263-4, and by Crane [1977], who has pointed out that the interpretation of the spectral data in terms of signal level probability distributions has proved difficult.

3.3 Spectral Broadening

Physically, spectral broadening arises because of Doppler shifting of the rf signal as it is scattered by moving irregularities. Spectral broadening observations are similar to intensity scintillations in that they respond to, and furnish information on, only small-scale fluctuations. With spacecraft signals, the closest distance to the Sun that can be usefully probed by both spectral broadening and intensity scintillations is set by signal-to-noise ratio considerations and these are more constraining for intensity scintillations [Woo and Armstrong, 1979]. In the case of Viking, spectral broadening was measured as close as 1.8 $R_\odot$ at 2.3 GHz and at 1.4 $R_\odot$ at 8.4 GHz. Examples of spectral broadening for one-way traversal

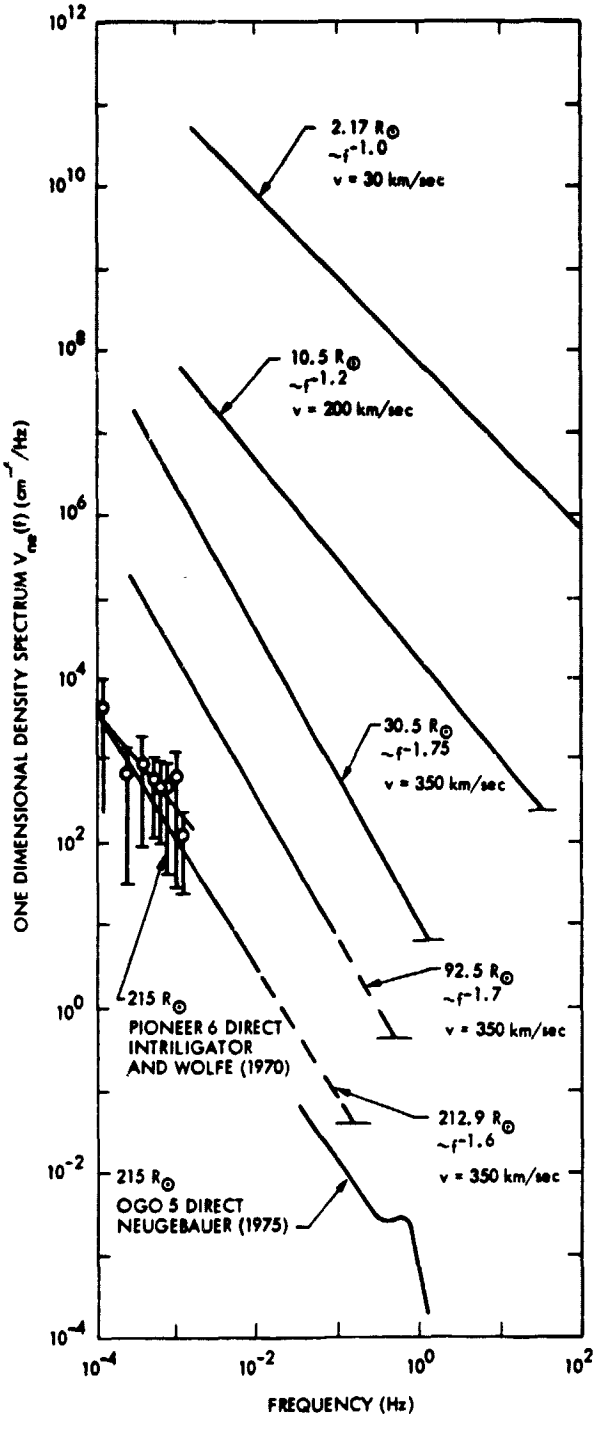

FIGURE 13

Typical one-dimensional electron density spectra v_{ne} deduced from Viking phase-difference scintillation spectra. Data marked A are in situ measurements from Pioneer 6 by Intriligator and Wolfe [1970], the curve marked B is from in situ measurements of OGO 5 by Neugebauer [1975]. (After Woo and Armstrong, 1979).

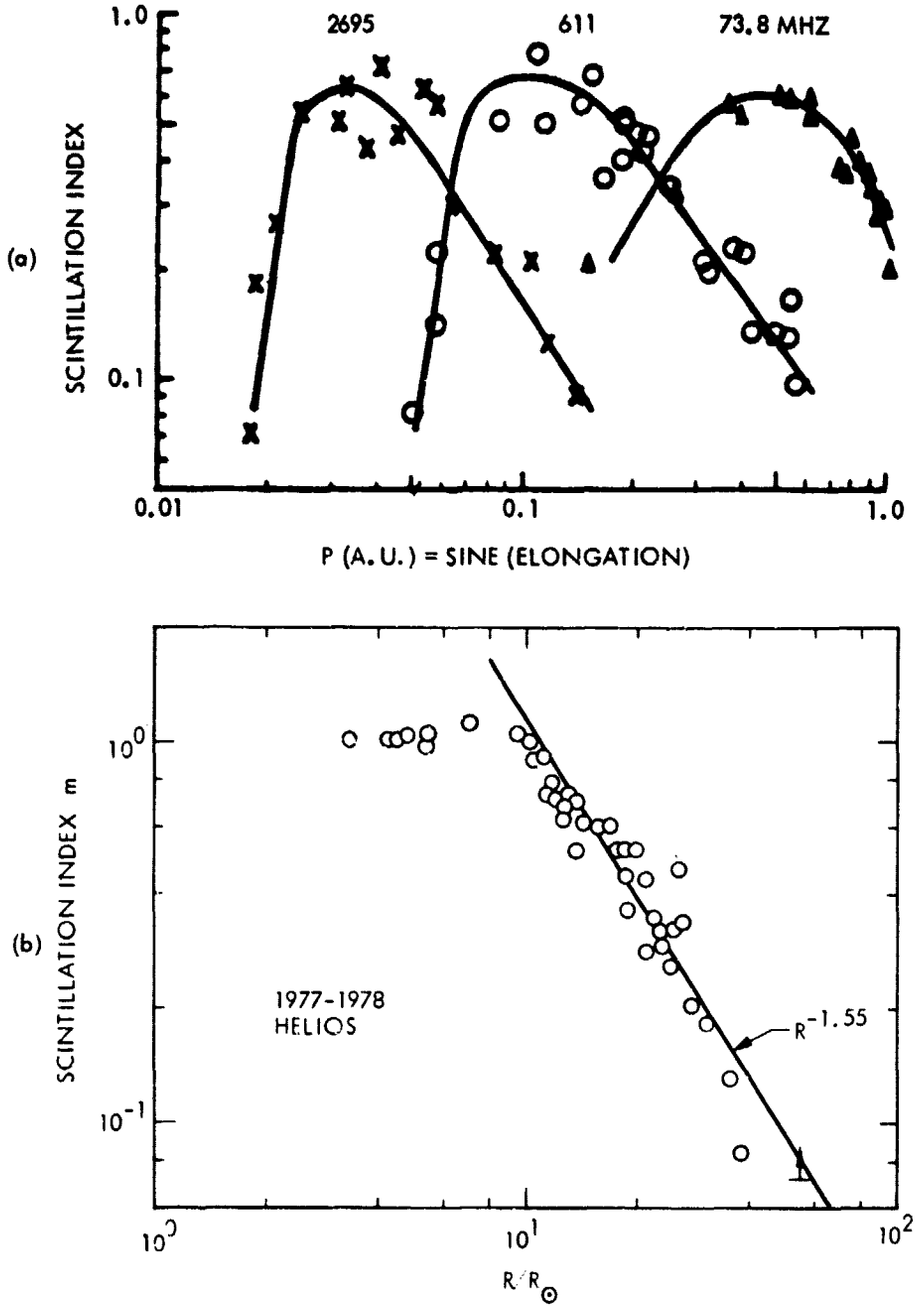

FIGURE 14

Behavior of the intensity scintillation index, m, for natural (extended) and spacecraft (point) radio sources. (a) The variation of scintillation index with distance from the sun for natural sources at three radio frequencies. (After Coles et al. 1974). (b) Intensity scintillation measurements of 2.3 GHz signal from Helios spacecraft received at Goldstone, California plotted as a function of nearest approach of the propagation path to the Sun (after Woo, 1979).

at 2.3 GHz are shown in Figure 15. The spectral broadening bandwidth B is defined as in Goldstein [1969]:

$$\int_0^B P(f)\ df = \frac{1}{2}\int_0^\infty P(f)\ df \qquad (20)$$

where P(f) is the spectrogram of the received signal. The radial variation of B with heliocentric distance at 2.3 GHz is given by Woo [1978]. Spectral broadening has a serious effect on performance on paths with small impact parameters.

3.4 Angular Broadening

Decrease in signal level at very close approach to the Sun was observed both for Pioneer 6 [Goldstein, 1969] and for Helios [Woo, 1978]. As was discussed in Section 2.1, the collision frequency in the plasma is still too low to account for this decrease through absorption, so it is attributed to the angular broadening of the signal from the spacecraft due to turbulence to the extent that it is larger than the beamwidth of the receiving antenna [Woo, 1978]. In the case examined, it amounted to 4.5 dB and was clearly a significant consideration.

3.5 Coherence Bandwidth

There appears to be few if any experimental results on phase and amplitude coherence of two monochromatic signals at different radio frequencies, but Woo [1975] has calculated the coherence functions for the X- and S-band cases. In these cases, coherence is maximum for signal fluctuation components of around 1 Hz.

3.6 Frequency Dependence

The frequency dependence for the homogeneous plasma parameters at microwave frequencies is determined by the simple asymptotic expression ($f \gg f_N$, $f \gg f_H$):

$$n \simeq 1 - \frac{X^2}{2} = 1 - \frac{1}{2}\frac{\omega_N^2}{\omega^2} = 1 - \frac{1}{2}\frac{f_N^2}{f^2} \qquad (21)$$

These values are summarized in Table III in the main text, and, with the exception of dispersion (f^{-3}), all vary with radio (carrier) frequency as f^{-2}.

The effects of inhomogeneities in the plasma present a more complicated picture as their frequency dependence is a function of the turbulence parameter, p. These dependencies for the rms behavior of the various parameters are summarized in Table V. While the values listed are basically theoretical, the values of p are derived from the measurements in Figure 13 where the exponent shown for $v_{ne}(f)$ is p-2. The value p = 11/3 is that corresponding to the Kolmogorov spectrum. A striking feature of Table V is that only for intensity scintillation does the exponent decrease in going from weak to strong scintillation.

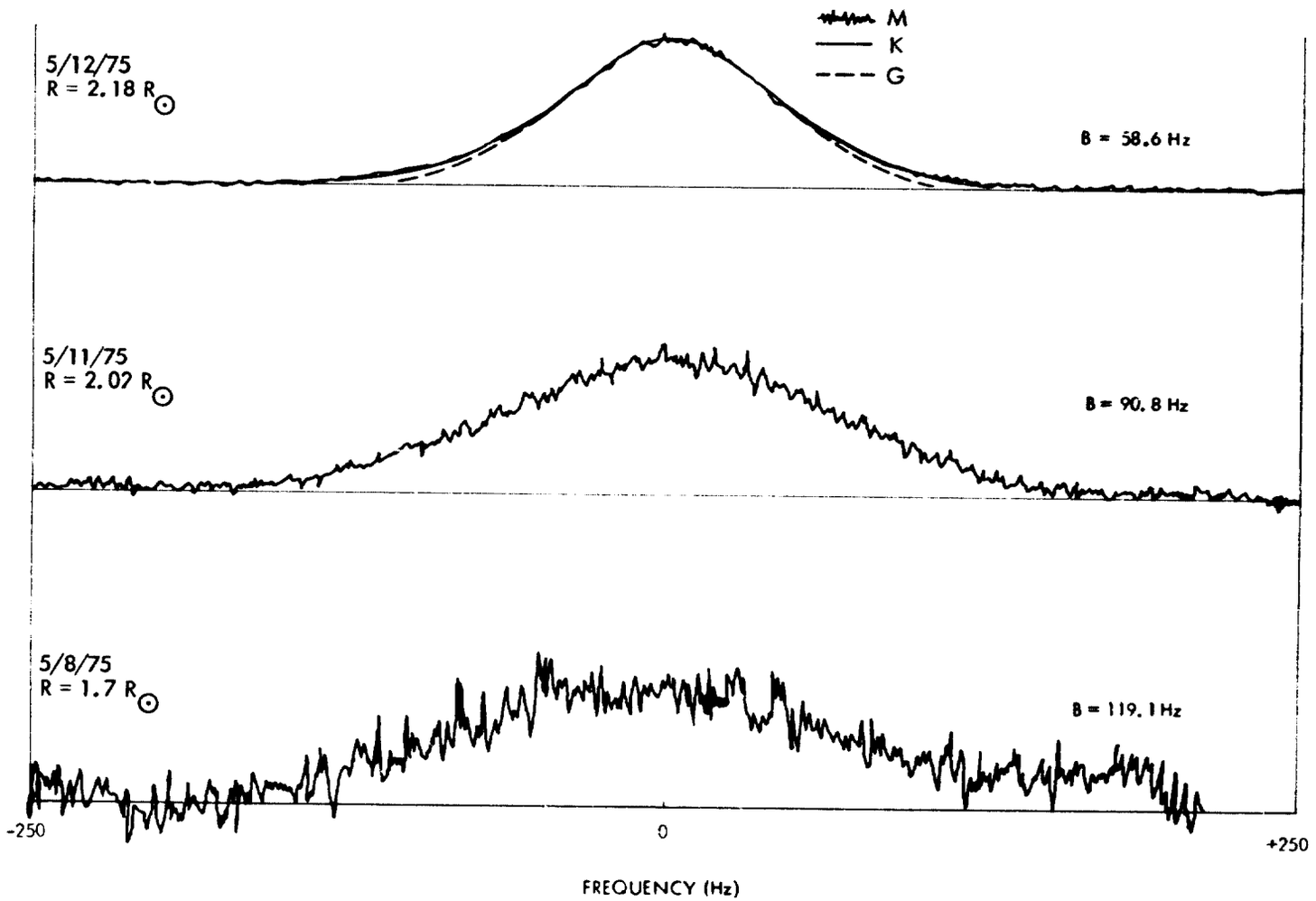

FIGURE 15

Three Helios spectrograms measured close to the Sun of the 2.3 GHz carrier frequency with a receiver bandwidth of 500 Hz. Spectral broadening bandwidth, B, is defined as in the text. In the top figure M = measurement, K = theory (Kolmogorov), and G = theory (Gaussian). (After Woo, 1978).

TABLE V

Frequency dependence of plasma turbulence effects in terms of the exponent y (effect $\sim f^y$ where f is the carrier frequency)

Effect	Parameter	Exponent y: Relation	Exponent y: Large Elongation ($R \geq 20\ R_\odot$) $p = 11/3$	Exponent y: Small Elongation ($R \leq 20\ R_\odot$) $p = 3$
Intensity scintillation[1]	m	$-\frac{p+2}{4}$	-1.42	-1.2
Phase scintillation[2]	σ_ϕ	-1.0	-1.0	-1.0
Spectral broadening[3]	B	$\frac{2}{2-p}$	-1.2	-2.0
Angular broadening[4]	θ	$\frac{p}{2-p}$	-2.2	-3.0

[1] Woo 1978, Woo et al., 1976a.

[2] Woo 1978.

[3] Woo and Armstrong 1978, Woo et al., 1976a.

[4] Woo et al., 1977.

SECTION III

MODELS OF EXTRATERRESTRIAL PLASMAS

1. INTRODUCTION

It is clear from the discussion in Section II that three characteristics of extraterrestrial plasmas that affect microwave signals are electron density N, the one-dimensional spectrum of rms electron density fluctuations v_{ne}, and the velocity of the plasma motion (ordered and thermal). The effects of the solar corona and solar wind tend to be common to all space missions and these two topics are therefore treated in some detail in Section III.2 and in Table VI. Space does not permit similar detail for each planet, so the principal features are tabulated in Table VII and references to some of the extensive literature on the subject are provided.

It is not efficient to completely separate the discussion of propagation effects and of the propagation medium. Therefore, one of the three important characteristics of the propagation medium mentioned above has already been covered in considerable detail. This is the one-dimensional spectrum of rms electron density fluctuations (v_{ne}) that is treated in Section II.3. Hence, the part on inhomogeneities in this Section is very brief.

2. THE SOLAR CORONA AND SOLAR WIND

The characteristic of the Sun and terminology associated with this discussion of the Sun are summarized in Table VI. To the extent possible, the numerical values have been made consistent with those given by Allen [1976].

2.1 Plasma Density

Berman [1979] has recently reviewed some 16 determinations by 11 authors of the solar wind (or extended corona) term of the Allen-Baumbach relation [Allen, 1976] for the electron density out to 1 AU. The model now recommended by Berman is:

$$N(R) \cong \frac{2.21 \times 10^{14}}{R^6} + \frac{1.55 \times 10^{12}}{R^{2.3}} \quad \text{electrons m}^{-3} \qquad (22)$$

In this model, the inner corona is modelled by the first term, which gives a value of $N = 1.25 \times 10^{14}$ m^{-3} at $R = 1.1\ R_\odot$, which agrees with Allen's [1976] model and becomes equal to the second term at $3.8\ R_\odot$. (For electron densities at lower solar altitudes, tabulated values should be used.) It yields a value at 1 AU ($214.94\ R_\odot$) of $N = 6.70 \times 10^6$ electrons m^{-3} which is in good general agreement with observations. Allen [1976] points out that the electron density in the solar wind at 1 AU varies inversely with velocity and reaches a maximum of about 8×10^7 m^{-3}.

TABLE VI

Characteristics and terminology of the sun

Heliographic equator:	The plane perpendicular to the Sun's rotation axis that divides its mass in two; the inclination of the solar equator to the ecliptic is 7°15'
Radius, $R_\odot$:	696,997 km
Rotation period: (sidereal)	25 days at equator 28 days at 40° heliographic latitude >28 days nearer the poles
Photosphere:	Visible disk of the Sun; it has a physical temperature of 6000 K at its base, and a minimum of 4150 K at 500 km above this base; the disk of the Sun subtends an angle at the Earth, which varies between 31'31" of arc and 32'35" of arc
Chromosphere:	Spherical shell of 2000 km thickness actually made up of about half a million small spikes called spicules with lifetimes of 5 to 15 minutes; the chromosphere appears to have a temperature of about 8000 K; all measures of solar radius, height in the corona, etc., are made from the base of the chromosphere [Allen, 1976]
Corona:	Faint white halo around the Sun, which becomes visible during an eclipse; it is at an effective temperature of 2 to 6 million K; the term also refers to the actual plasma of electrons and ions in the upper solar atmosphere; the base of the corona may be taken as the transition region at 1.003 $R_\odot$; the outer boundary is not clearly defined but is commonly taken at 6 $R_\odot$ [Yakovlev, 1974]
Solar wind	The expansion of the corona into space; the corona contains areas that are particularly cool and quiet, known as coronal holes; many astronomers feel that the solar wind emanates from these holes; the solar wind originates inside the corona and is terminated at a few tens of AU by an interaction with the interstellar magnetic field [Brandt, 1970]; the solar wind velocity near the Earth is ~450 km/s and the average density at 1 AU is 5 to 10 x 10^6 m^{-3}; the magnetic field associated with the solar wind is initially radial but may be directed either inwards or outwards; a region of like-directed field is known as a sector

TABLE VI (Continued)

Coronal holes:	Regions of diverging magnetic field of the corona, which appear dark when viewed in soft X-ray images, in white light comographs, and in eclipse photographs of the solar corona; coronal holes are always sources of high-speed solar wind streams; because coronal holes tend to last longer than one solar rotation, there is a 27-day recurrence period for high-speed streams at the Earth, producing a natural explanation for the well-known recurrence period in geomagnetic activity [Bartels, 1934], and the associated source at the Sun, which has up until this discovery been known as an "M-Region" [Suess, 1979].

TABLE VII

Properties of planetary atmospheres and ionospheres[1]

Item/Planet	Mercury	Venus	Earth	Mars	Jupiter	Saturn	Uranus	Neptune	Pluto
Mean distance from Sun (AU)[2]	0.387	0.723	1	1.524	5.203	9.539	19.18	30.06	39.44
Known satellites	0	0	1	2	14	10	5	2	0
Main atmospheric components	None (traces of He, O, C etc.)	90-97% carbon dioxide	Nitrogen, oxygen	Carbon dioxide	Hydrogen, helium	Hydrogen, helium	Hydrogen, helium, methane	Hydrogen, helium, methane	None detected
Mean temperature at visible surface (degrees Celsius) S = solid, C = clouds	350 (S) day -170 (S) night	-33 (C) 480 (S)	22 (S)	-23 (S)	-150 (C)	-180 (C)	-210 (C)	-220 (C)	-230 (?)
Atmospheric pressure at surface (millibars)	10^{-9}	90,000	1,000	6	700	?	?	?	?
Surface gravity (Earth = 1)	0.37	0.88	1.0	0.38	2.64	1.15	1.17	1.18	?
Ionosphere	Some trapped electrons	Well developed	D, E, F1, F2	Yes	Yes				
Maximum electron density (el per m^3)	?	10^{11} to 10^{12}	2×10^{12}	10^{11}	2×10^{11} (day) 2×10^{10} (night)				
Height of maximum electron density (km)	?	150-200	250-400	125	1600 (day) 2300 (night)				
Magnetic field	Yes - weak	Yes - weak	Yes - strong	Yes - weak	Yes - strong	Yes - strong			
Magnetic dipole moment (G cm^3)	1.8 to 6 x 10^{22}	2 to 6.5 x 10^{22}	8 x 10^{25}	2.5 x 10^{22}	1.55 x 10^{30}	2 x 10^{29}	?	?	?
Dipole:quadrapole: octopole ratios			1:00:0.14:0.1		1.0:0.25:0.2				

[1] Sagan [1975], Pasachoff [1977], Russell [1979], and others.

[2] The astronomical unit (the mean distance from the Earth to Sun) is 1.496 x 10^8 km.

Expression (22) is appropriate to low heliographic latitudes (±15°). Allen [1976] and Saito, et al., [1977] both find a decrease in electron density by a factor of 4 to 5 between the equator and pole for the inner corona. Tyler, et al., [1977] propose a model including a simple expression to account for variation with heliographic latitude (θ), which has been modified slightly here to fit the above observations:

$$N(\theta) \sim \left(\cos^2 \theta + \frac{1}{25} \sin^2 \theta\right)^{1/2} \tag{23}$$

This expression may be used in connection with (22) if desired. As N(0) = 1 no adjustment of (22) is necessary. Its appropriateness is questionable for $R > 5\ R_\odot$.

It is now believed that the solar wind and, hence most interplanetary plasma, originates in coronal holes. A survey of models of coronal hole flows has recently been published by Suess [1979], while Holzer [1978] has written a review of the solar wind and related phenomena, which has been cast in the context of coronal holes. A general review of coronal holes and high-speed wind streams has been published by Zirker [1977].

While substantial variation of plasma density with solar cycle is known to exist, these variations have yet to be sufficiently understood to be incorporated into models. For the time being, it is suggested that expression (22) be used for electron densities near the plane of the ecliptic, supplemented by expression (23) for higher heliographic latitudes for $R < 5\ R_\odot$, and that solar cycle variations be ignored.

2.2 Inhomogeneities

Fluctuations in radial electron density have been characterized in terms of the one-dimensional frequency spectrum V_{ne} (measured in situ by spacecraft) by Woo and Armstrong [1979]. Their determination is:

$$V_{ne}(f) = 5.2 \times 10^{10}\ R^{-3.45}\ f_s^{-1.65}\ v^{-1}\ \frac{(\text{electrons/cm}^3)^2}{\text{Hz}} \tag{24}$$

and, if the solar wind speed v is assumed to be 3×10^5 m/s and constant:

$$V_{ne}(f) = 1.5 \times 10^{5}\ R^{-3.45}\ f_s^{-1.65}\ \frac{\text{electrons/cm}^3}{\text{Hz}} \tag{25}$$

where R is in solar radii ($20 \leq R \leq 215$), f_s is the fluctuation frequency in Hz, and v is the solar wind speed in m/s.

For values of $R < 20\ R_\odot$, one can interpolate values of the V_{ne} from Figure 13.

2.3 Velocity and Temperature

The velocity vector follows the spiral defined by the rotation of the Sun and the frozen-in magnetic field [Brandt, 1970]. A recent scintillation

analysis indicates that the average radial component of the solar wind velocity for distances less than 1 AU from the sun is given by

$$V_r(r) = \left[\frac{440}{r^{-0.3} + 3.35 \times 10^{-7}\, r^{-4.0}} \right] \quad \text{km/second} \qquad (26)$$

where r is the radial distance in AU.

There is a direct relationship between velocity and geomagnetic activity such that a velocity of 400 km/s is associated with very quiet and v = 700 km/s with very disturbed geomagnetic conditions [Allen, 1976].

3. PLANETARY IONOSPHERES AND MAGNETOSPHERES

This section discusses the four inner planets (Mercury, Venus, Earth, and Mars) and the nearest (and largest) of the outer planets, Jupiter. At present these are the planets for which data from spacecraft visitations are available. Summary information is found in Table VII. The atmospheric information is drawn from Sagan [1975], and Pasachoff [1977]. Information on planetary ionospheres is taken from the sources referenced in the texts on the various planets in this section and its associated figures.

3.1 Mercury

Mercury, the innermost planet, has one of the least hospitable surface environments, due to its close proximity to the Sun. The maximum angle from the Sun at which Mercury can be viewed from the Earth is only 28° so that it is never seen optically against a really dark sky. Until recently astronomers believed the rotation period of Mercury to be the same as its period of revolution about the Sun, namely 88 days. This would have meant that one half of the planet was always in sunlight, the other half always in dark. However, radar measurements from the Arecibo Observatory indicate the rotation period to be 59 days. Thus the spin-orbit coupling, instead of exhibiting a ratio of 1:1 has a ratio of 2:3. Further information may be found, for example, in Murray [1975] and Pasachoff [1977].

The existence of a magnetic field on Mercury has been established and electrons and traces of atmospheric gases observed. The planet exhibits a bow shock and magnetopause similar to that of the Earth, but both are severely compressed in the direction of the Sun.

3.2 Venus

Venus is covered by clouds from about 30 km above the surface to an altitude of 80 km. The visible surface of these clouds at around 60 km exhibit a temperature of around 240 K at a pressure of around 200 mb. From this level, the temperature increases monotonically to a value of about 750 K on the solid surface, at which point the pressure has risen to 90 bars. The clouds of Venus give the planet an apparent rotation period of about four days [Young and Young 1975], while radar measurements of the solid surface put the rotation period at 243 days. The difference can be explained by postulating wind velocities in the cloud layer of up to 100 meters per second. Good discussions are found in Young and Young [1975], Pasachoff [1977], and Colin, et al., [1979].

Electron densities of 5×10^{11} el m^{-3} have been measured at altitudes of 150-180 km above the solid surface [Knudsen, et al., 1979]. The ionization is found to stay about 10^{10} el m^{-3} for ionopause heights of 1500 km, and then to drop sharply above the ionopause. The principal positive ion above 180 km is O^+ and below 180 km it is O_2^+ [Taylor, et al., 1979]. Some of the measured data on Venus is given in Figure 16. The maximum electron density shown corresponds to a plasma frequency of 6.3 MHz [Kliore, et al., 1979]. The magnetic field has been estimated to be very weak [Russell, 1979].

3.3 The Earth

The ionosphere of the Earth up to an altitude of 2000 km is described in detail in Report 725, while the effects of Earth-space propagation out to the geostationary orbit at 6.6 Earth radii measured from the center of the Earth (6.6 $R_\oplus$) are given in Report 263-4. In this section, the terminology necessary to distinguish ionization connected to the Earth from that of the solar wind is given.

The Earth's plasma environment is shown in Figure 17 [Van Allen, 1975]. This environment is strongly influenced by the Earth's magnetic field represented by a dipole moment of 8×10^{25} gauss cm^{-3} inclined 11° to the axis of rotation.

3.3.1 Plasmasphere

This region of relativity high electron densities (10^9 to 10^{10} electrons m^{-3}) at low intermediate geomagnetic latitudes is contained along closed lines of geomagnetic force. In the equatorial plane, the plasmapause occurs between 5 and 6 $R_\oplus$ and defines an asymmetrical torus outside of which the electron density is 10 to 100 times less than inside. The location of the plasmapause is strongly influenced by magnetic activity.

3.3.2 Magnetosphere

In this region, the Earth's plasma is controlled by the geomagnetic field. The boundary between the ionosphere and magnetosphere is taken by some authors to lie at altitudes of 500 to 2000 km above the surface, while other authors choose not to distinguish the regions. The magnetopause is the outer boundary of the magnetosphere and is seen to be compressed on the day side of the Earth and extended on the night side.

3.3.3 Bow shock

The bow shock separates the undisturbed supersonic solar wind from the bow-shaped shock wave that lies between it and the magnetosphere. The electron density in the solar wind impinging on the Earth's bow shock is approximately 5 to 10×10^6 el m^{-3}. As in all plasmas, electric neutrality is maintained so there are an equal number of positive ions.

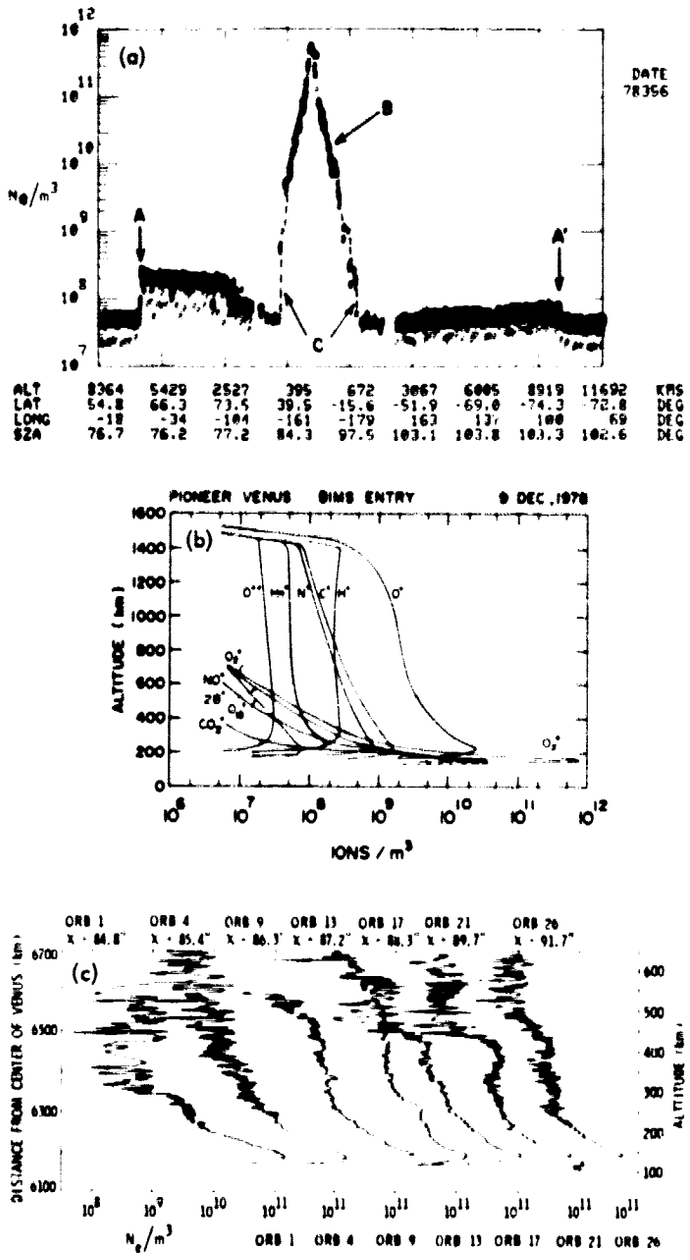

FIGURE 16

The ionosphere of Venus from Pioneer Venus measurements. (a) Electron density measurements acquired by the orbiter electron density probe on 1978 day 356, showing the bow shock, A, A', and the ionosphere, B. (After Brace et al. 1979); (b) Ion composition during entry near dawn local time (Taylor et al. 1979); (c) A series of electron density measurements of orbits 1, 4, 9, 13, 17 and 21. The profiles are staggered by one decade, and the 10^5 cm^{-3} level is indicated for each profile. The solar zenith angle (x) for each orbit is indicated on the upper horizontal axis. (Kliore et al. 1979).

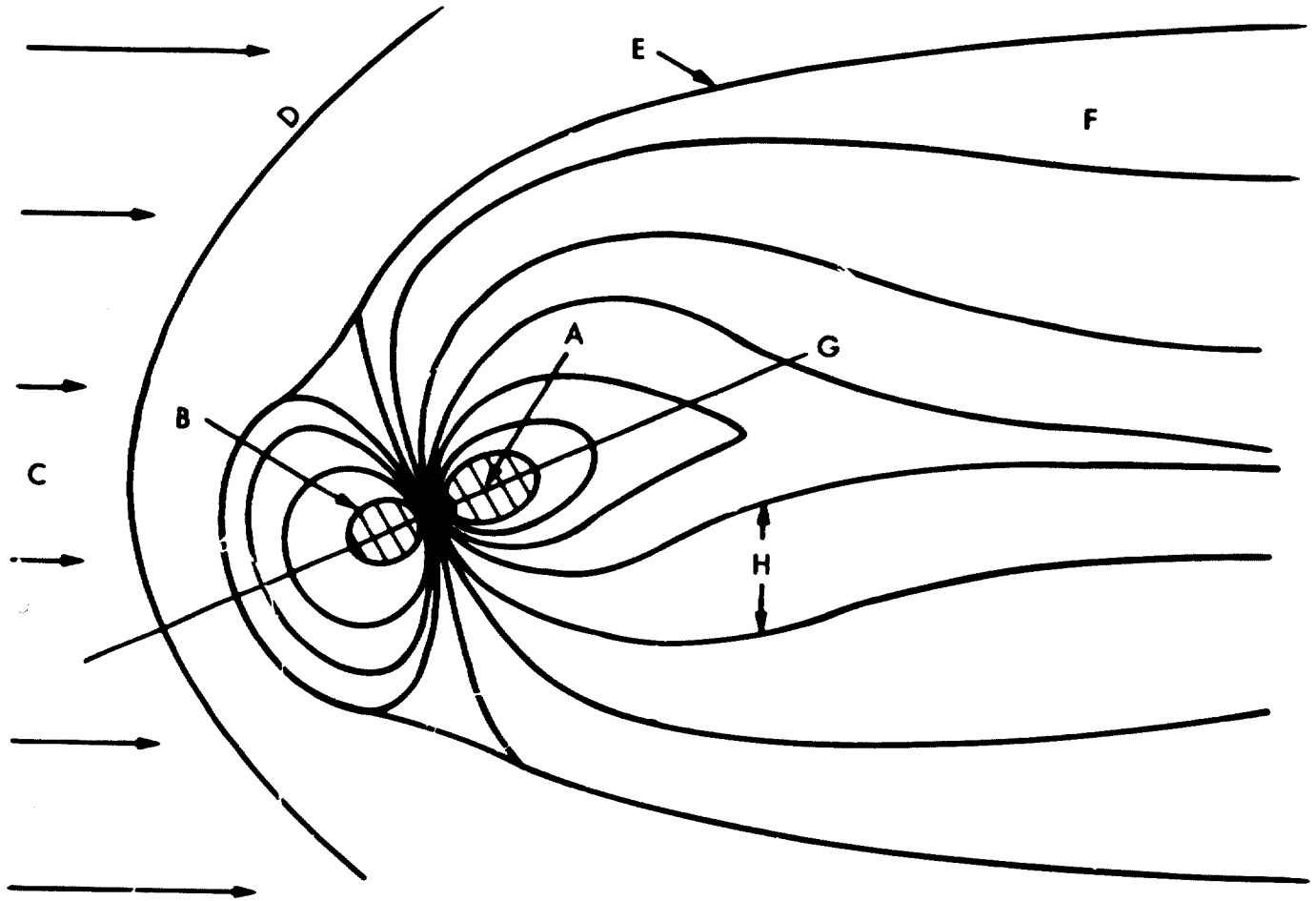

FIGURE 17

The structure of the Earth's magnetosphere showing the location of the plasmasphere (A), the plasmapause (B), solar wind (C), bow shock (D), magnetopause (E), magnetosphere (F), geomagnetic equator (G), and magnetic field lines (H). (After Van Allen, 1975).

3.4 The Moon

The Moon is the most massive planetary satellite in the solar system in relation to its planetary partner. It is without atmosphere or ionosphere The Moon's mean distance from the Earth, about 380,000 km (or about 60 $R_\oplus$), and its orbital inclination are such that the Moon moves through the tail of the Earth's magnetosphere once a month at full Moon.

3.5 Mars

Mars is a small planet only about half the diameter of Earth. The Martian atmosphere is about one percent that of the Earth (around 6-mb pressure at the surface), and is 90-percent carbon dioxide. The surface temperature is below freezing (-23°C) and there is, in fact, little water vapor in the atmosphere. The Martian magnetic field is very weak (see Table VII).

Shown in Figure 18 are two sets of measurements (Vikings 1 and 2) of the ionosphere of Mars [Hanson, et al., 1977]. The peak electron density (5×10^{11} m^{-3}) corresponds to a plasma frequency at 2.85 MHz and is significantly less than that of the Earth's F-region.

3.6 Jupiter

Jupiter, the largest of the planets, dominates the Sun's planetary system at a distance of 5 AU. It revolves around the Sun once every 11.9 years. Its volume is 1400 times that of Earth, but its mass is only 318 times as great (its density is only 1.3 g/cm^3). It rotates very rapidly (once every 10 hours). Jupiter's atmosphere is 85-percent hydrogen molecules and 15-percent helium, plus traces of methane and ammonia. There are at least 14 moons, four of them (discovered by Galileo) of a size comparable to the planet Mercury: Io, Europa, Ganymede, and Callisto [e.g., Wolfe, 1975].

That Jupiter has a strong magnetic field and radiation belts similar to the Earth was deduced from noise bursts emanating from Jupiter and measured on Earth by Burke and Franklin [1955] at 22 MHz. Since then, Jupiter has received a lot of attention from radio astronomers primarily at decametric wavelengths [see Kraus, 1966]. Recent measurements of the Jovian ionosphere are shown in Figure 19.

3.7 Other

The planets Saturn, Uranus, Neptune, and Pluto are not covered in this report, other than the sketchy statistics included in Table VII. The Pioneer Venus spacecraft encountered Saturn in September of 1979, and new information on that planet is expected shortly. Scientific American [1975] offers general information on the outer planets.

Comets offer an interesting future area for spaceflight study. The tail of a comet first becomes visible about 1.7 AU from the Sun [Allen, 1976] and frequently separates into two distinct components: an ion tail that is always pointed away from the sun, and a dust tail that curves along the comet's parabolic trajectory around the Sun [Pasachoff, 1977].

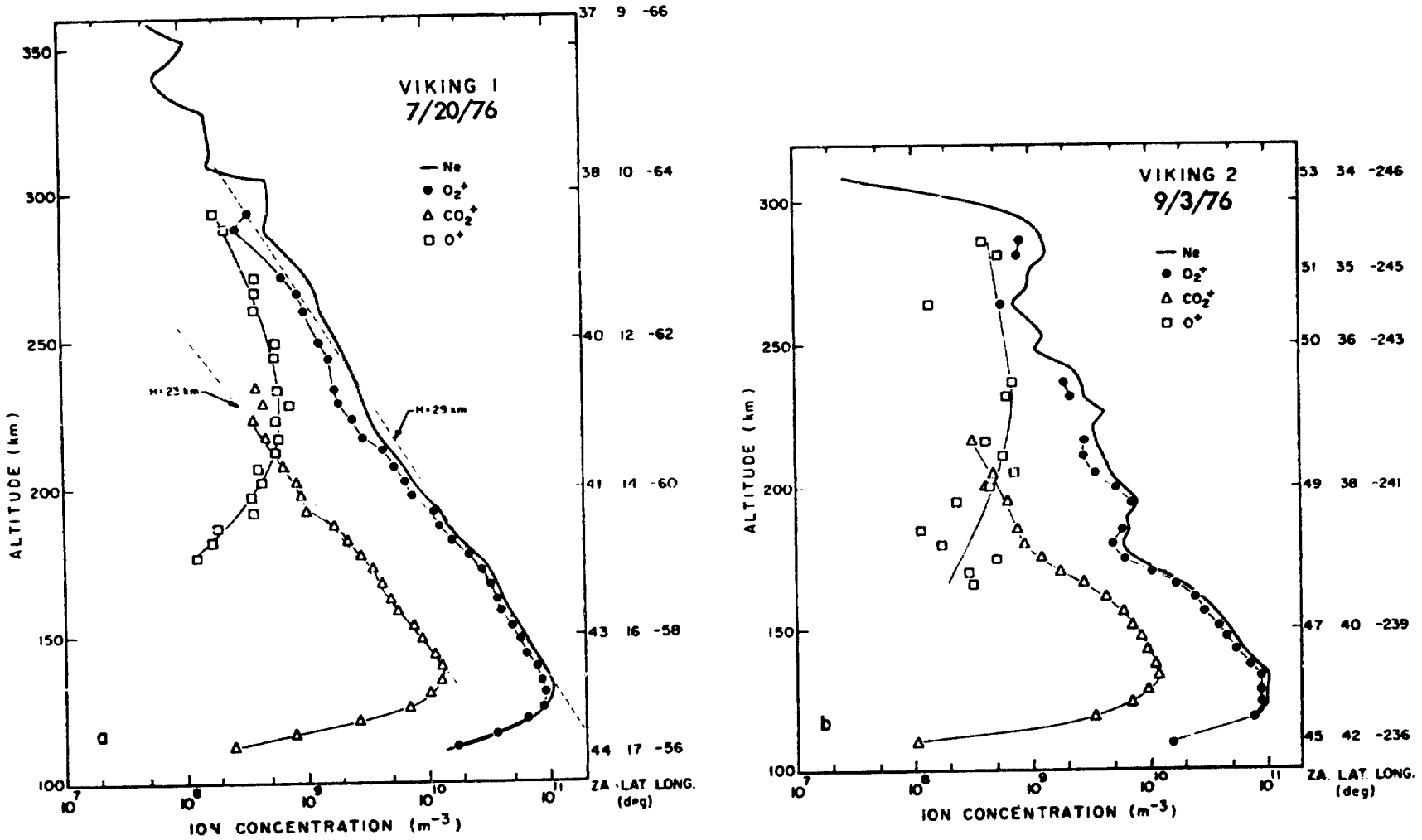

FIGURE 18

The Martian ionosphere. Plots of the observed electron density (N_e) and positive ion densities. (After Hanson et al. 1977)

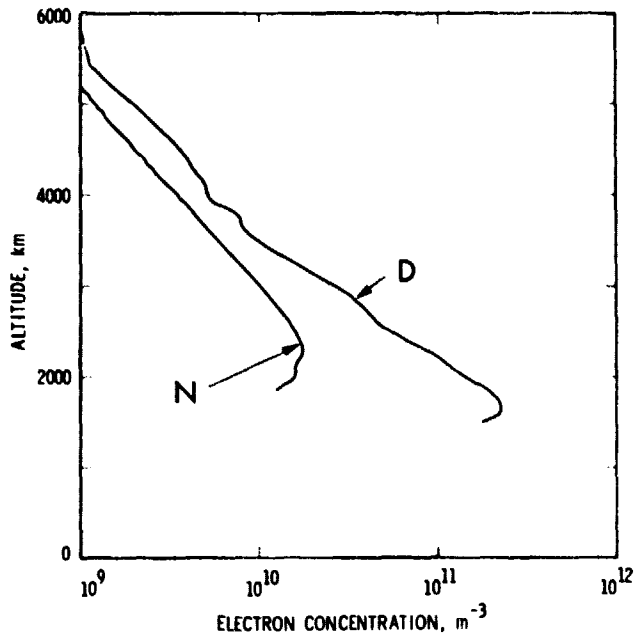

FIGURE 19

Two measurements of the ionosphere of Jupiter from Voyager 1. The ingress measurement (D) is daytime and the egress (N) is night. (After Eshleman et al. 1979).

REFERENCES

ALLEN, C.W. [1976] Astrophysical Quantities, The Athlone Press, University of London.

ANDERSON, J.S., and F. B. Estabrook [1979] Application of DSN spacecraft tracking technology experimental gravitation, J. Spacecraft and Rockets 16, 120-125 (March/April)

BARTELS, J. [1934] Twenty-seven day recurrences in terrestrial magnetic and solar activity, 1923-1933. J. Geophys, Res. 39, 201-202.

BERMAN, A.L. [1979] A unified observational theory for solar wind columnar turbulence. Deep Space Network Progress Report 42-50 Jan./Feb. 1979, pp. 743-808 (23 Feb.)

BOOKER, H.G. [1934] Some general properties of the formulae of the magneto-ionic theory. Proc. Roy. Soc. A., 147-352

BOOKER, H.G. [1975] Electromagnetic and hydromagnetic waves in a cold magneto-plasma, Phil. Trans. Roy. Soc. Lond A 280, 57-93.

BRACE, L.H. et al., [1979] Electron temperature and densities in the Venus ionosphere: Pioneer Venus Orbiter electron temperature probe results. Science 203, 763-765 (23 Feb. 1979).

BRANDT, J.C. [1970] Introduction to the solar wind. W. H. Freeman and Co., San Francisco.

BUDDEN, K.G. [1961] Radio Waves in the Ionosphere. Cambridge, at the University Press.

BURKE, B.F. and FRANKLIN, K.L. [1955] Observations of a variable radio source associated with the planet Jupiter. J. Geophys. Res. 60, 213-217 (June).

CALLAHAN, P.S. [1975] Columnar content measurements of the solar wind turbulence near the sun. Ascrophys. J., 199, 227-236 (1 July).

CCIR REPORTS: Recommendations and Reports of the CCIR, 1978, XIV Plenary Assembly, Kyoto, 1978; International Radio Consultative Committee, International Telecommunication Union, Geneva, 1978 (available from NTIS).

- Report 222-4, Effects of plasmas on communications with spacecraft, Vol. II, pp. 77-90.

- Report 536-1, Telecommunication requirements for manned and unmanned deep-space research, Vol. II, pp. 119-132.

- Report 683, Preferred frequency bands for deep-space research using manned and unmanned spacecraft, Vol. II, pp. 132-143.

- Report 720, Radio emission associated with absorption by atmospheric gases and precipitation, Vol. V, pp. 103-106.

- Report 725, Ionospheric properties, Vol. VI, pp. 1-12.

COATES, R.J. [1969] Tracking and data acquisition for space exploration. Space Science Reviews 9, 361-418. D. Reidel Publishing Company, Dortrecht, Holland.

COHEN, M.H. [1969] High resolution observations of radio sources. Annual Rev. Astron. and Astrophys, 7, 619-664.

COLES, W.A. [1978] Interplanetary scintillations, Space Sci. Rev. 21, 411.

COLES, W.A., RICKETT, B.J., and RUMSEY, V.H., [1974] Interplanetary scintillations. Solar Wind Three, C.T. Russell, Ed. Published by the Institute of Geophysics and Planetary Physics, University of California, Los Angeles, 90024.

COLES, W.A. and HARMON, J.K. [1978] Interplanetary scintillation electron density measurements of the electron density power spectrum in the solar wind. J. Geophys. Res., 81, 1413.

COLES, W.A., RICKETT, B.J., and SCOTT, S.L., [1978] Scintillation observations near the Sun, pp. 388-396 of A closeup of the Sun, eds. M. Neugebauer and R.W. Davis. JPL Publication 78-70 (Sept. 1), Jet Propulsion Laboratory, California Institute of Technology, Pasadena, California.

COLIN, L. et al., [1975] Encounter with Venus (plus 25 associated articles on the ionosphere, atmosphere and surface of Venus). Science 203, No. 4382, pp. 743-808 (23 Feb. 1979).

CRANE, R.K. [1977] Ionospheric Scintillation. Proc. IEEE 65, 180-199 (Feb.)

DAVIES, K. [1968] Ionospheric Radio Waves. Blaisdell Publishing Co., Waltham, Mass.

EASTERLING, M.F. [1964] Chapters 5 and 6 of Digital Communications. Prentice Hall, Englewood Cliffs, New Jersey, U.S.A.

EDELSON, R.E., MADSEN, B.D., DAVIS, E.K., and GARRISON, G.W. [1979] Voyager telecommunications: the broadcast from Jupiter. Science 204, 913-921 (1 June 1979)

ESHLEMAN, V.R., TYLER, G.L., WOOD, G.E., LINDAL, A.F., ANDERSON, J.D., LEVY, G.S. and CROFT, T.A. [1979] "Radio Science with Voyager 1 at Jupiter: Preliminary profiles of atmosphere and ionosphere." Science 204, 976-978 (1 June 1979)

GARRIOTT, O.K., da ROSA, A.V., and ROSS, W.J. [1970] Electron content obtained from Faraday rotation and phase path length variations. J. Atmos. Terr. Phys. 32, 705-728 (April)

GINZBURG, V.L. [1967] Propagation of electromagnetic waves in plasma. Moscow, Nauka

GOLDSTEIN, R.M. [1969] Superior conjunction of Pioneer Venus. Science 166, 598

HANSON, W.B., SANATANI, S., and ZUCCARO, D.R., [1977] The Martian ionosphere as observed by the Viking potential analyzers. J. Geophys. Res. 82, 4351-4363.

HERMAN, J.R. and GOLDBERG, R.A. [1978] Sun, weather, and climate. NASA SP-426

HEWISH, A., SCOTT, P.F., and WILLIS, D., [1964] Interplanetary scintillation of small diameter radio sources. Nature 203, 1214

HOLZER, T.E., [1978] The solar wind and related astrophysical phenomena. Solar System Plasma Physics: A Twentieth Anniversary Overview, C.F. Kennel, L.J. Lanzerotti, and E.N. Parker, eds., North-Holland Publishing Co.

INTRILIGATOR, D.S. and WOLFE, J.H. [1970] Preliminary power spectra of the interplanetary plasma. Astrophys. J. 162, L187.

JOKIPII, J.R. [1973] Turbulence and scintillations in the interplanetary plasma. Ann. Rev. Astron. Astrophys. 11, 1.

KLIORE, A.V., WOO, R., ARMSTRONG, J.W., PATEL, I.R., and CROFT, T.A. [1979] The polar ionosphere of Venus near the terminator from early Pioneer Venus Orbiter radio occultations. Science 203, 765-768 (23 Feb.)

KNUDSEN, W.C., SPENNER, K., WHITTEN, R.C., SPREITER, J.R., MILLER, K.L., and NOVAK, V. [1979] Thermal structure and major ion composition of the Venus ionosphere: first RPA results from Venus orbiter. Science 203, 757-763 (23 Feb.)

KOLOSOV, M.A., SOKOLOV, A.V., and YAKOVLEV, O.I. [1979] Investigation of radio wave propagation in the solar system. IEEE Trans. Ant. and Prop., Vol. AP-27, No. 1, 18-22 (Jan.)

KRAUS, J.D., [1966] Radio Astronomy. McGraw Hill Book Co.

LEVY, G.S., SATO, T., SEIDEL, B.L., STELZREID, C.T., OHLSON, J.E., and RUSCH, W.V.T. [1969] Pioneer 6: measurements of transient Faraday rotation phenomena observed during solar occultation. Science, Vol. 166, 596-598 (31 Oct.)

MELBOURNE, W.G., [1976] Navigation between the planets. Scientific American 234, 58-74 (June)

MICHAEL, W.H. et al. [1977] The Viking radio science investigations. J. Geophys. Res. 82, 4293.

MURRAY, B.C., [1975] Mercury. Scientific American, Sept. 1975, pp. 37-48

NEUGEBAUER, J. [1975] The enhancement of solar wind fluctuations at the proton thermal gyroradius. J. Geophys. Res. 80, 998.

PASACHOFF, J.M. [1977] Contemporary Astronomy. W.B. Saunders Co.

PARKER, E.N. [1963] Interplanetary Dynamical Processes. Interscience Publishers

RATCLIFFE, J.A. [1959] The Magneto-ionic Theory and its Applications to the Ionosphere. Cambridge, at the University Press.

RISHBETH, H. and GARRIOTT, O.K. [1969] Introduction to Ionospheric Physics. Academic Press, New York and London.

RUSSELL, C.T. [1979] Planetary magnetism. Rev. Geophys. and Sp. Phys. 17, 295-301, (April)

SAGAN, C. [1975] The solar system. Scientific American, Sept. 1975, pp. 1-11.

SAITO, K., POLAND, A.J., and MUNRO, R.H. [1977] A study of the background corona near solar minimum. Solar Physics 55, 121-234.

SCIENCE: Special issues. Vol. 203, No. 4382 (23 Feb. 1979): Encounter with Venus, Vol. 204, No. 4396 (1 June 1979): Voyager 1 encounter with the Jovian system, Vol. 205, No. 4401 (6 July 1979): Pioneer Venus results.

SCIENTIFIC AMERICAN [1975] Special issue on the Solar system (September)

SHKAROFSKY, I.P., JOHNSON, T.W., and BACHYNSKI, M.P. [1966] Particle kinetics of plasmas. Addison Wesley Publishing Co.

STELZRIED, C.T. [1970] A Faraday rotation measurement of a 13-cm signal in the solar corona. Jet Propulsion Laboratory, Technical Report 32-1401, July 15, 1970.

STELZRIED, C.T., LEVY, G.S., SATO, T., RUSH, W.V.T., OHLSON, J.E., SCHATTEN, K.H., and WILCOX, J.M. [1970] The quasi-stationary coronal magnetic field and electron density as determined from a Faraday rotation experiment. Solar Physics 14, 440-456.

STIX, T.H. [1962] Theory of Plasma Waves. McGraw-Hill Book Company.

SUESS, S.T. [1979] Models of coronal hole flows. Space Science Reviews 23, 159.

TAYLOR, H.A., et al. [1979] Ionosphere of Venus: First observations of the day side ion composition near dawn and dusk. Science 203, 752-754 (23 Feb.).

TYLER, G.L., BRENKLE, J.P., KOMAREK, T.A., and ZYGIELBAUM, A.I. [1977] The Viking solar corona experiment. J. Geophys. Res. 82, 435-4340 (Sept. 30)

VAN ALLEN, J.A. [1975] Interplanetary particles and fields. Scientific American, Sept. 1975, pp. 127-136

VOLLAND, H., BIRD, M.K., LEVY, G.S., STELZREID, C.T., and SEIDEL, B.L. [1977] Helios-1 Faraday rotation experiment: results and interpretations of the solar occultations in 1975. J. Geophys. 42, 659-672

WAIT, J.R. [1968] Electromagnetics and Plasmas. Holt, Rinehart and Winston, Inc.

WOLFE, J.H. [1975] Jupiter. Scientific American, Sept. 1975, pp. 95-104

WOO, R. [1975] Multifrequency techniques for studying interplanetary scintillations. Astrophys. J. 201, 238-248 (1 Oct.)

WOO, R. [1977] Measurements of the solar wind using spacecraft scattering observations. Study of Travelling Interplanetary Phenomena, M.A. Shea, et al., eds., pp. 81-100. D. Reidel Publishing Co., Dordrecht, Holland.

WOO, R. [1978] Radial dependence of the solar wind properties deduced from Helios 1, 2, and Pioneer 10, 11 radio scattering observations. Astrophys. J. 219, 727-739

WOO, R [1979] Spacecraft radio scintillation and scattering measurements of the solar wind. To be published in Solar Wind 4, ed. H. Rosenbauer, Springer-Verlag

WOO, R., and ARMSTRONG, J.W. [1979] Spacecraft radio scattering observations of the power spectrum of electron density fluctuations in the solar wind. J. Geophys. Res. (in press)

WOO, R., YANG, F.C., and ISHIMARU, A. [1976a] Structure of density fluctuations near the sun deduced from Pioneer 6 spectral broadening measurements. Astrophys. J. 218, 557

WOO, R., YANG, F.C., YIP, K.W., KENDALL, W.B. [1976b] Measurements of large-scale density fluctuations in the solar wind using dual frequency phase scintillations. Astrophys. J. 210, 568

WOO, R., YANG, F.C., and ISHIMARU, A. [1977] Probing the solar wind with radio measurements of the second moment field. Astrophys. J. 218, 577-568 (1 Dec.)

YAKOVLEV, O.I. [1974] Radio Wave Propagation in the Solar System, NASA TT F-15, 723. Translation of Rasprostraneniye Radiovoln v Solnechnoy Sisteme, Moscow, "Sovetskoye Radio" Press, 1974, 192 pp.

YEH, K.C., and LIU, C.H. [1972] Theory of ionospheric waves. Academic Press, New York and London.

YOUNG, A., and YOUNG, L., [1975] Venus. Scientific American, Sept. 1975, 49-58.

ZIRKER, J.B. [1977] Coronal holes and high speed wind streams. Rev. Geophys. and Space Phys. 15, pp. 257-269.

APPENDIX

AUTHORIZING TEXTS OF CCIR STUDY GROUP 6

At the CCIR XIV Plenary Assembly, Kyoto, 1978, the terms of reference for Study Group 6 (Propagation in ionized media) were expanded, a Question was broadened, and a Study Programme was approved to include propagation through extraterrestrial ionized media. In CCIR usage the Question and Study Programme are defined as follows:

Question: A Statement of a technical or operational problem, to which an answer is required.

Study Programme: Text describing the work to be carried out on a technical or operational problem constituting the subject of a Question.

The specific wording approved at the 1978 Plenary Assembly is:

Terms of reference (for Study Group 6, Propagation in ionized media) to study:

1. the propagation of radio waves through the ionosphere, and through ionized regions beyond the ionosphere;

2. the characteristics of radio noise;

with the object of improving telecommunications.

QUESTION 25/6

IONOSPHERIC PROPERTIES

The CCIR, (1978)

CONSIDERING

that ionized media affect the propagation of radio waves,

UNANIMOUSLY DECIDES that the following question should be studied:

what are the properties of the ionosphere and other ionized media which affect propagation in ways that are important to radio systems?

Note. - See Reports 250-4, 262-4, 340-3, 725, 726 and Recommendations 373-4, 434-3.

STUDY PROGRAMME 25E/6

RADIO PROPAGATION THROUGH THE SOLAR
AND OTHER EXTRA-TERRESTRIAL IONIZED MEDIA

The CCIR, (1978)

CONSIDERING

(a) that a simple model of the ionized solar atmosphere and the ionospheres of the planets would provide a basis for propagation studies needed to support the planning of space flights near the sun and the planets;
(b) that simple models of the extra-terrestrial plasma would provide a similar basis for deep-space flights,

UNANIMOUSLY DECIDES that the following studies should be carried out:

1. determination of the characteristics of the ionized solar atmosphere, the ionospheres of the planets and their associated effects on radio propagation;
2. determination of the characteristics and effects of the extra-terrestrial plasma pertinent to radio propagation over interplanetary to intergalactic distances.